Short Title: Role of BST4 in Chlamydomonas

Title: The role of BST4 in the pyrenoid of *Chlamydomonas reinhardtii*

Authors: Liat Adler[1,2,], Chun Sing Lau[3], Kashif M. Shaikh[4], Kim A. van Maldegem[4], Alex L. Payne-Dwyer[3,5], Cecile Lefoulon[6], Philipp Girr[3], Nicky Atkinson[1,2], James Barrett[3], Tom Z. Emrich-Mills[3], Emilija Dukic[4], Michael R. Blatt[6], Mark C. Leake[3,5], Gilles Peltier[7], Cornelia Spetea[4], Alistair J. McCormick[†,1,2], Luke C. M. Mackinder[†3], Charlotte E. Walker[†3]

[1]Institute of Molecular Plant Sciences, School of Biological Sciences, University of Edinburgh, EH9 3BF, United Kingdom.

[2]Centre for Engineering Biology, University of Edinburgh, EH9 3BF, United Kingdom.

[3]Centre for Novel Agricultural Products (CNAP), Department of Biology, University of York, Heslington, York YO10 5DD, United Kingdom.

[4]Department of Biological and Environmental Sciences, University of Gothenburg, Gothenburg 40530, Sweden.

[5]School of Physics, Engineering and Technology, University of York, Heslington, York YO10 5DD, United Kingdom.

[6]Laboratory of Plant Physiology and Biophysics, Bower Building, University of Glasgow, Glasgow, United Kingdom.

[7]Aix-Marseille Université, CEA, CNRS, Institut de Biosciences et Biotechnologies Aix-Marseille, CEA Cadarache, 13108 Saint-Paul-lez-Durance, France

[†]The author(s) responsible for distribution of materials integral to the findings presented in this article in accordance with the policy described in the Instructions for Authors (https://academic.oup.com/plcell/pages/General-Instructions) are:

- Alistair McCormick, School of Biological Sciences, University of Edinburgh, +44 1316 505316, alistair.mccormick@ed.ac.uk
- Luke Mackinder, Department of Biology, University of York, +44 1904 328984, luke.mackinder@york.ac.uk
- Charlotte Walker, Department of Biology, University of York, +44 1904 328500, charlotte.walker@york.ac.uk

One-sentence summary: In Chlamydomonas, the pyrenoid-localized bestrophin-like protein BST4 is a putative ion channel involved in pH regulation of the thylakoid lumen.

Funding information: This work was funded by the Biotechnology and Biological Sciences Research Council (BBSRC) (grant number (BB/S015531/1) and Leverhulme Trust (RPG-2017-402). LA acknowledges funding support by EASTBIO DTP (BB/J01446X/1). CEW acknowledges funding support from BBSRC Discovery Fellowship (BB/W009587/1). CSL was supported by Bill & Melinda Gates Agricultural Innovations (Investment ID 53197). CS acknowledges grants from the Swedish Research Council (VR 2016-03836 and 2021-03790). KMS was recipient of a postdoctoral fellowship from the Carl Tryggers Foundation (CTS 20:406). A United Kingdom Research and Innovation Future Leaders Fellowship to LCMM (MR/T020679/1), Biotechnology and Biological Sciences Research Council grants (BB/T017589/1, BB/S015337/1, BB/R001014/1) and Engineering and Physical Research Council Grant (EP/W024063/1) with ML and APD. The authors would like to thank the University of York Biosciences Technology Facility for confocal microscopy access and support. CL was funded by BBSRC grants BB/P011586/1 and BB/T013508/1 to MRB. PG was supported by the Deutsche Forschungsgemeinschaft (DFG, German Research Foundation) – project number 456013262.

ABSTRACT

The eukaryotic algal CO_2-concentrating mechanism (CCM) is based on a Rubisco-rich organelle called the pyrenoid, which is typically traversed by a network of thylakoid membranes. BST4 is a bestrophin-like transmembrane protein that has previously been identified in the model alga *Chlamydomonas reinhardtii* as a putative tether that could link the traversing thylakoid membrane network to the Rubisco matrix. In the present study, we show that BST4 forms a higher order complex assembly that localizes to the thylakoid network within the pyrenoid. However, investigation of a *bst4* knock-out mutant in Chlamydomonas showed that the absence of BST4 did not result in a CCM-deficient phenotype and that BST4 is not necessary for the formation of the trans-pyrenoid thylakoids. Furthermore, heterologous expression of BST4 was not sufficient to facilitate the incorporation of thylakoids into a reconstituted Rubisco condensate in the land plant Arabidopsis. Subsequent analyses revealed that *bst4* was under oxidative stress and showed enhanced non-photochemical quenching

67 associated with CO_2 limitation and over acidification of the thylakoid lumen. We
68 conclude that the primary role of BST4 is not as a tethering protein, but rather as an
69 ion channel involved in pH regulation in pyrenoid-based CCMs.

70 **INTRODUCTION**

71 Maintaining improvement in crop yields to keep pace with the rising demands for food
72 is becoming increasingly challenging (Horton et al., 2021). A possible solution to
73 overcome this challenge is engineering a biophysical CO_2 concentrating mechanism
74 (CCM) into C3 crop plants, which has the potential to improve crop yields by up to
75 60% as well as water-use and nitrogen-use efficiency (Price et al., 2013; McGrath and
76 Long, 2014; Long et al., 2019; Fei et al., 2022; Wu et al., 2023). The biophysical CCMs
77 in algae typically function by concentrating CO_2 into a Rubisco-rich, liquid-liquid phase
78 separated microcompartment called a pyrenoid. This raises the $[CO_2]$:$[O_2]$ ratio around
79 the primary CO_2-fixing enzyme Rubisco, which brings Rubisco closer to its maximal
80 carboxylation rate and minimizes the competing oxygenation reaction.
81 *Chlamydomonas reinhardtii* (hereafter Chlamydomonas) has the most well
82 understood pyrenoid-based CCM and has become the blueprint for engineering such
83 a CCM into C3 plants (Hennacy and Jonikas, 2020; Adler et al., 2022).

84 An important yet little understood aspect of the Chlamydomonas CCM is the function
85 and biogenesis of the thylakoid tubule network that traverses the pyrenoid (Engel et
86 al., 2015). The pyrenoid tubules are continuous with the thylakoid membrane and are
87 thought to function as a delivery system for inorganic carbon (Ci) to the Rubisco matrix.
88 In the current model, bicarbonate (HCO_3^-) is channelled into the thylakoid lumen by
89 bestrophin-like proteins 1-3 (BST1-3) and diffuses to the pyrenoid tubules where it is
90 converted to CO_2 by carbonic anhydrase 3 (CAH3) (Karlsson et al., 1998; Mukherjee
91 et al., 2019; Burlacot et al., 2022). Association of the condensed Rubisco to the
92 thylakoid membrane is predicted to be essential for an efficient CCM. Therefore,
93 understanding the mechanisms of pyrenoid tubule formation will be crucial (Fei et al.,
94 2022).

95 The protein BST4 (bestrophin-like protein 4, also known as Rubisco binding
96 membrane protein 1, RBMP1; Cre06.g261750) localizes exclusively to the pyrenoid
97 tubules and has been proposed to function as a tether protein, linking the Rubisco
98 matrix to the tubules (Meyer et al., 2020). BST4 is a predicted transmembrane protein

99 and has two Rubisco binding motifs (RBMs) on its long, disordered C-terminus (Fig.
100 1A) (He et al., 2020; Meyer et al., 2020). RBMs facilitate the targeting of proteins to
101 the pyrenoid and are also hypothesized to underpin the assembly of the pyrenoid.
102 Meyer et al. (2020) proposed that BST4, together with other tether proteins, may
103 recruit Rubisco to the tubule network.

104 BST4 also has a well-conserved bestrophin domain similar to those present in the
105 thylakoid-localized BST1-3 proteins (Mukherjee et al. 2019). Bestrophins primarily act
106 as anion channels and are found in a wide diversity of organisms, including animals,
107 plants and fungi. They are best known to have permeability to chloride and HCO_3^- (Qu
108 and Hartzell, 2008), although some are reportedly permeable to cations (Yang et al.,
109 2014) and larger organic anions (Roberts et al., 2011). It is possible that BST4
110 functions as an HCO_3^- channel, like that proposed for BST1-3 (Mukherjee et al. 2019),
111 but there are currently no data to support this hypothesis.

112 In this study we aimed to elucidate the role of BST4 in the Chlamydomonas CCM. We
113 tested BST4 as a thylakoid-Rubisco tethering protein as well as its suitability in
114 promoting a thylakoid-Rubisco matrix interface in the model land plant Arabidopsis.
115 We also explored an alternative hypothesis that BST4 functions as an ion channel in
116 the pyrenoid tubules and discussed the implications this has for our current
117 understanding of CO_2 fixation by the pyrenoid.

118 RESULTS AND DISCUSSION

119 BST4 is a bestrophin-like protein that is localized in the intra-pyrenoid thylakoid 120 tubules in Chlamydomonas

121 The amino acid sequence of BST4 has two key unique features compared to BST1-3.
122 (Fig. 1), the latter of which play a key role in Ci uptake in the CCM (Mukherjee et al.
123 2019). First, BST4 has an extended disordered C-terminus that contains two RBMs
124 (Fig. 1A) (He et al., 2020; Meyer et al., 2020). Second, BST4 has a phenylalanine
125 residue in the first position of the putative selection pore, as opposed to valine which
126 is conserved throughout BST1-3 (Fig.1B, C). In corroboration, we found the
127 evolutionary history of BST4 to be distinct from BST1-3 when investigated using
128 maximum likelihood phylogenetic analysis. We analysed the full-length sequence (Fig.
129 S1) and a truncated version without the disordered C-terminal, leaving the bestrophin

domain and N-terminal (Fig. 1D), both of which found BST4 to resolve in a distinct clade from BST1-3 but within the wider green algae group.

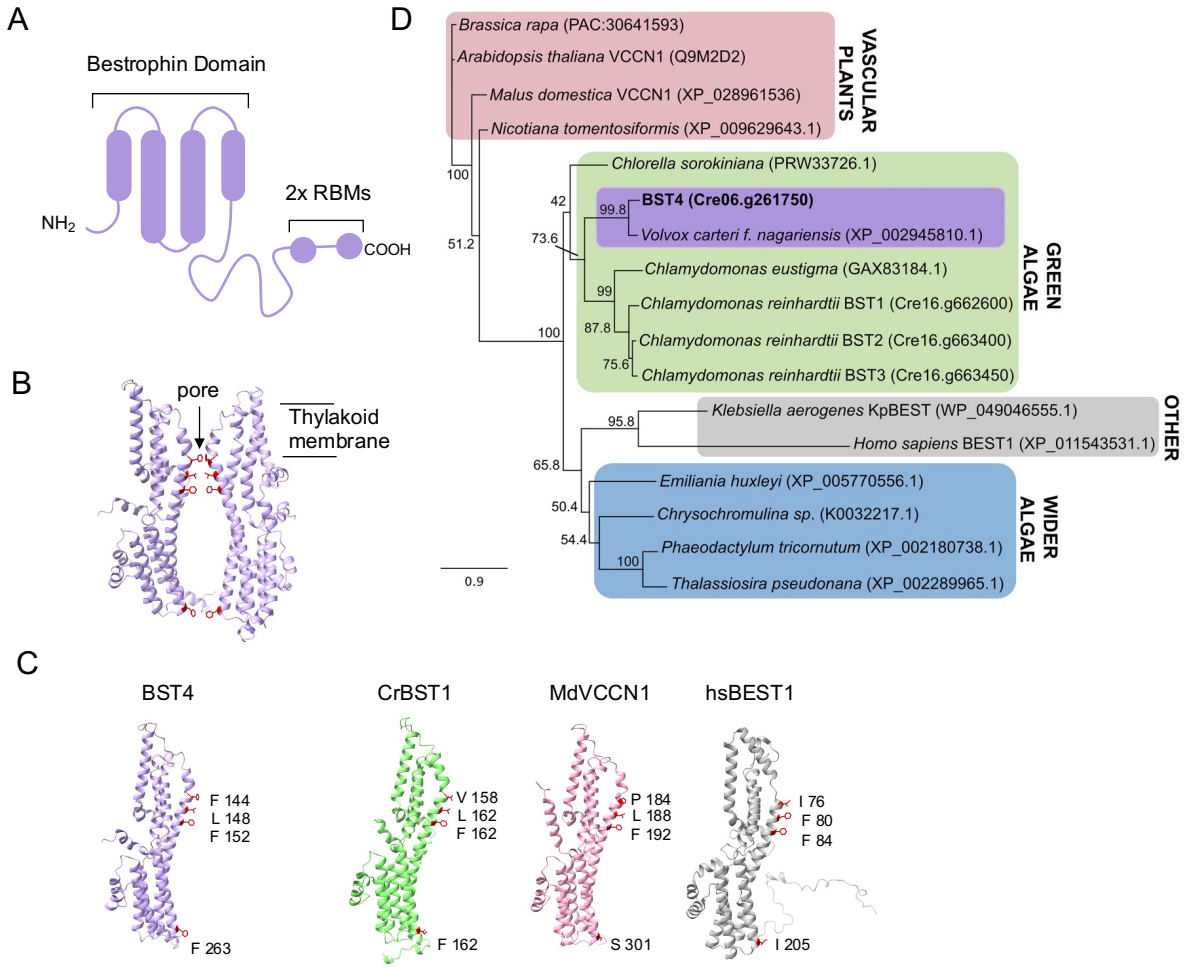

Figure 1. BST4 is a bestrophin protein that is distinct from BST1-3. A. Schematic of the topology of BST4. BST4 is predicted to have four transmembrane domains and a disordered C-terminus containing two Rubisco Binding Motifs (RBMs) **B.** AlphaFold models of two BST4 bestrophin domains (amino acid residues 53-386 shown for clarity) to show a typical bestrophin channel pore. Pore lining residues are highlighted in red. **C.** AlphaFold structures of the BST4 bestrophin domains alongside structures of bestrophins from *Chlamydomonas reinhardtii* (*Cr*BST1; Alphafold), *Malus domestica* (*Md*VCCN1;7EK1) and *Homo sapiens* (*Hs*BEST1; 8D1I). Residues known to line the channel pore are highlighted. **D.** Phylogenetic analysis of the BST4 bestrophin domain (bold) with the disordered C-terminal removed. The alignment used was trimmed at residue 369. The evolutionary history of BST4 was inferred by using the maximum likelihood method based on the Le and Gascuel substitution model with discrete Gamma distribution (5 categories) and 500 bootstrap replicates. The tree is drawn to scale, with branch lengths measured in the number of substitutions per site.

As well as being distinct at a sequence level, BST4 also localizes differently from BST1-3. While BST1-3 localize throughout the thylakoid membrane and are enriched at the pyrenoid periphery (Mukherjee et al., 2019), BST4 localizes to the centre of the pyrenoid in a pattern that resembles the pyrenoid thylakoid tubule system (Fig. 2A, B; Meyer et al., 2020). To confirm tubule localisation, we generated a dual-tagged line that expressed BST4-mScarlet-I and the Chlamydomonas Rubisco small subunit 1

150 (*Cr*RBCS1) fused to Venus. BST4-mScarlet-I was enriched where *Cr*RBCS1-Venus
151 was depleted (Fig. 2C, D), indicating that BST4 is located in the tubules and not the
152 Rubisco-enriched pyrenoid matrix. Nevertheless, previous work has shown that the C-
153 terminal RBMs of BST4 enable the protein to interact with *Cr*RBCS1 (Meyer et al.
154 2020). We confirmed using a yeast-2-hybrid approach that the C-terminus of BST4
155 interacts with *Cr*RBCS1 (Fig. S2A). We also measured the efficiency of Förster
156 resonance energy transfer (FRET) from Venus to mScarlet-I, and found that the FRET
157 efficiency was ~35%, supporting the proximity of *Cr*BST4 to *Cr*RBCS1 (Fig. S2B).

158 Bestrophins typically form pentameric assemblies (Bharill et al., 2014; Hagino et al.,
159 2022). To investigate if this is the case for BST4, we initially used an AlphaFold-
160 multimer modelling approach. When five chains of BST4 were inputted to AlphaFold
161 a pentameric structure was predicted (Fig. 2E). To test the complex assembly of BST4
162 *in vivo*, we utilized a Slimfield microscopy molecular tracking method (Plank et al.,
163 2009). We first developed a Chlamydomonas line that only expressed fluorescently
164 tagged BST4 by expressing BST4-mScarlet-I in a *bst4* mutant background (Fig. S3).
165 We then tracked individual fluorescent molecules of BST4-mScarlet-I and quantified
166 the number of BST4 monomers per complex. The resulting probability distribution
167 revealed that the most common BST4 complex is made up of five molecules (Fig. 2F).
168 Other peaks showed complexes with numbers of molecules divisible by five, which
169 may be multiple pentameric channels grouping together. The interval between the
170 probability peaks was also five (Fig. 2G). To further support higher order complex
171 assembly of BST4 we ran purified Chlamydomonas thylakoid membranes on a Blue
172 Native-PAGE gel (BN-PAGE) and immunoblotted for BST4 (Fig. 2H). BST4 formed a
173 smear at ~1000 kDa, which is considerably larger than a pentamer (~330kDa). This
174 could be due to higher order assemblies of BST4, pentameric BST4 in a complex with
175 other proteins and/or aberrant migration during BN-PAGE due to influences by
176 complex shape. Collectively, our data support *in vivo* higher order assembly of BST4
177 potentially as a pentamer.

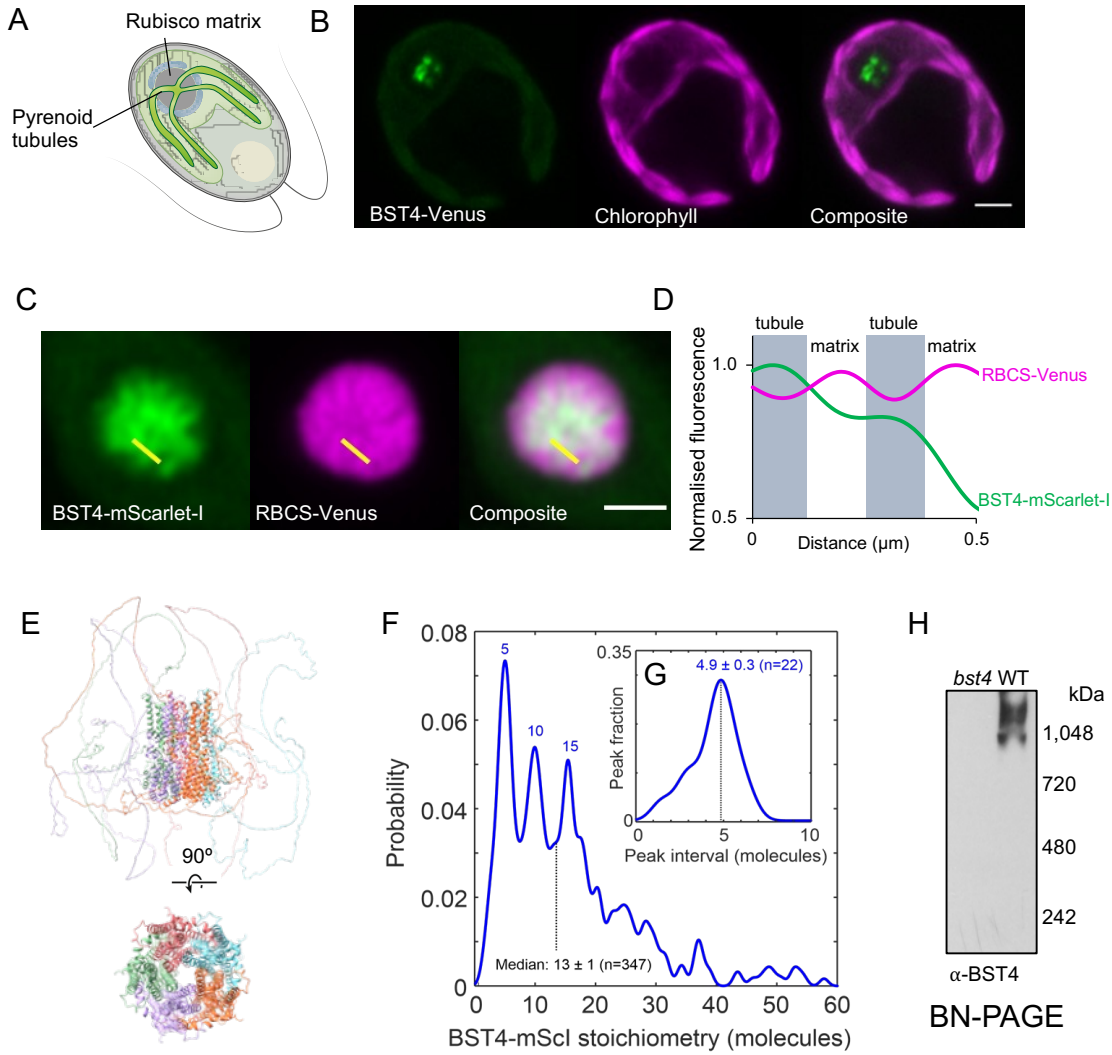

Figure 2. BST4 forms higher order assemblies in the pyrenoid tubules in Chlamydomonas. A. Diagram of a Chlamydomonas cell with the pyrenoid Rubisco matrix and pyrenoid tubules indicated. **B.** Confocal image of a Chlamydomonas cell expressing BST4-Venus. Scale bar is 2 µm. **C.** Pyrenoid in dual-tagged Chlamydomonas. BST4-mScarlet-I and RBCS-Venus are shown in green and magenta, respectively. Overlap appears white. The yellow line shows the 1D cross-section used for generating the line plot in (D). Scale bar is 1 µm. **D**. Plot of normalized fluorescence intensity values from a 1D cross-section from (C). mScarlet-I and RBCS-Venus are shown in green and magenta, respectively. **E**. AlphaFold prediction of pentameric BST4 structure. Top structure includes the disordered C-terminus, bottom structure displays amino acid residues 53-386 only for clarity. **F**. BST4-mScarlet-I stoichiometry probability distribution based on single particle tracking and molecular counting in live Chlamydomonas (n=347 tracks) using Slimfield microscopy. **G**. Averaging the intervals between peaks in BST4-mScarlet-I stoichiometry (n=22 intervals) indicates a consistent pentameric unit. **H**. Immunoblot of proteins from *bst4* mutant and wild type (WT) Chlamydomonas thylakoids separated by Blue Native-PAGE.

BST4 localizes to the stroma lamellae thylakoid membrane in Arabidopsis

We used Arabidopsis as a heterologous system to examine if BST4 was able to tether the Rubisco matrix to thylakoid membranes. In previous work, an Arabidopsis Rubisco small subunit (*At*RBCS) double mutant (*1a3b*) was complemented with *Cr*RBCS2,

195 resulting in a line with hybrid Rubisco representing ~50% of the Rubisco pool ($S2_{Cr}$)
196 (Izumi et al., 2012; Atkinson et al., 2017). Subsequent expression of the pyrenoid linker
197 protein Essential PYrenoid Component 1 (EPYC1), in $S2_{Cr}$ resulted in the formation of
198 an EPYC1-hybrid Rubisco condensate or 'proto-pyrenoid' (Atkinson et al., 2020). The
199 $S2_{Cr}$ line was therefore used as a platform to test whether BST4 acts as a tether
200 protein.

201 We initially localized a BST4-mNeon fusion protein following stable expression in $S2_{Cr}$
202 (Fig. 3). BST4-mNeon was observed in chloroplasts, demonstrating that the native
203 chloroplast signal peptide was compatible with the chloroplast targeting mechanism in
204 land plants (Fig. 3A), as seen previously for other Chlamydomonas proteins (Atkinson
205 et al., 2016). The fluorescence signal from BST4-mNeon had a sponge-like pattern
206 that was inversely correlated with the punctate chlorophyll autofluorescence signal that
207 represents the grana stacks (Fig. 3B, C). The sponge-like pattern was similar to
208 previous observations of autofluorescence originating from Photosystem I (Hasegawa
209 et al., 2010), which is enriched in the stroma lamellae of thylakoids. We subsequently
210 generated a stable Arabidopsis transgenic line expressing untagged BST4 to confirm
211 its location by biochemical fractionation. BST4 was detected in the thylakoid fraction
212 and not in the stromal fraction (Fig. 3D). The thylakoids were then further fractionated
213 into grana stacks and stroma lamellae sub-fractions. BST4 was found in the stroma
214 lamellae fraction (Fig. 3E), which is consistent with the observed sponge-like
215 fluorescence pattern.

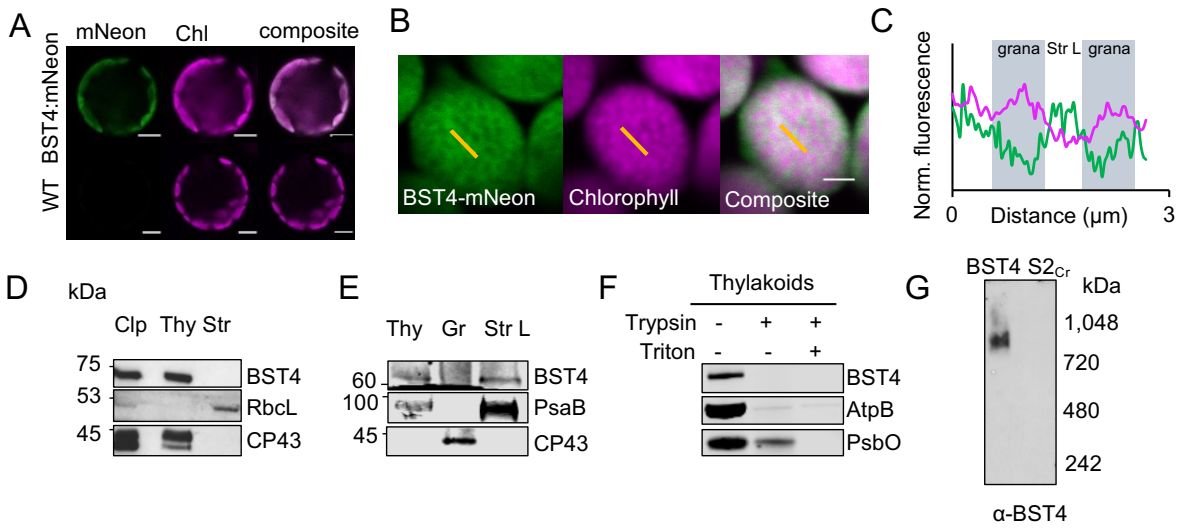

216

Figure 3. BST4 assembles as a complex in the stroma lamellae of thylakoids in Arabidopsis. A. Confocal image of WT protoplasts expressing BST4-mNeon. Scale bar is 5 µm. **B.** Mesophyll chloroplast from $S2_{Cr}$ Arabidopsis expressing BST4-mNeon. BST4mNeon and chlorophyll autofluorescence are shown in green and magenta, respectively. Overlap appears white. Scale bar is 2 µm. Yellow lines indicate selections for profile plot in (C). **C.** Plot of normalized fluorescence intensity values from a 1D cross-section (yellow line) through two grana stacks from (B). mNeon and chlorophyll autofluorescence are shown in green and magenta, respectively. **D.** Immunoblots of sub-chloroplast fractions isolated from Arabidopsis line $S2_{Cr}$ expressing BST4. RbcL and CP43 were probed for as stromal and thylakoid controls, respectively. **E.** Immunoblots of fractionation thylakoids from Arabidopsis line $S2_{Cr}$ expressing BST4. CP43 and PsaB were used for grana stack and stroma lamellae controls, respectively **F.** Trypsin protease protection assay. Intact thylakoids containing BST4 subjected to 0 or 100 µg/ml trypsin with or without the addition of 1% (v/v) Triton. AtpB and PsbO used as controls for stromal facing (exposed) and lumen facing (protected), respectively. **G.** Immunoblot of proteins from thylakoids separated by Blue Native-PAGE from either BST4 stable line or $S2_{Cr}$ background. Abbreviations: Clp, whole chloroplast; CP43, CP43-like chlorophyll binding protein; RbcL, Rubisco large subunit; PsbO, photosystem II manganese-stabilizing polypeptide;AtpB, ATP synthase subunit beta; PsaB, photosystem I P700 chlorophyll a apoprotein A2; Str, stromal fraction; Thy, thylakoid fraction.

As BST4 has two RBMs on its C-terminus, we hypothesized that BST4 should be orientated with the C-terminus facing the stroma so that the RBMs are available to interact with *Cr*RBCS. To determine the orientation of BST4, we performed a protease protection assay on thylakoids isolated from the untagged BST4 transgenic plants. Our antibody was raised against the C-terminal end of BST4, so it could be used to assess whether the C-terminus was exposed for degradation in the stroma or if it was protected in the lumen. We found that the BST4 C-terminus was fully degraded after a 60 min treatment of trypsin, indicating that it faced the stroma (Fig. 3F). There was some degradation of the lumenal control, PsbO, which we attribute to a portion of the thylakoid membrane preparation not being fully intact. However, PsbO was fully degraded when the membranes were solubilized, indicating that they were sufficiently intact to differentiate between lumenal- and stromal-facing peptides. Therefore, BST4 was observed in the expected location and orientation in plant thylakoid membranes.

Finally, we also tested whether BST4 forms a complex in the Arabidopsis thylakoid membrane. We subjected thylakoids from the untagged BST4 transgenic plants to BN-PAGE and detected a single band of ~850 kDa (Fig. 3G). Thus, BST4 forms a similar order complex in Arabidopsis to that in Chlamydomonas but may be lacking additional interaction partners present in Chlamydomonas.

BST4 is not sufficient for integration of thylakoids into the Arabidopsis proto-pyrenoid

To test whether BST4 could facilitate incorporation of thylakoids into hybrid Rubisco condensates (i.e., proto-pyrenoids) in plants, BST4-mCherry and EPYC1-tGFP were co-expressed in the $S2_{Cr}$ background (Fig. 4). When we expressed EPYC1 alone,

256 Rubisco condensates formed in chloroplasts as expected (Atkinson et al., 2020),
257 which were visible as a ~2 µm wide puncta in the tGFP channel (Fig. 4A). When BST4-
258 mCherry and EPYC1-tGFP were co-expressed, approximately 60% of the BST4-
259 mCherry fluorescence signal was observed in the condensate region (Fig. 4B, D), with
260 the remaining signal exhibiting the same sponge-like pattern as seen in Fig. 3A.

261 To confirm that the observed co-localisation was due to an interaction between BST4
262 and *Cr*RBCS2, we mutated the first two residues of each core RBM motif of BST4 to
263 glutamic acid (WR to EE). Previously, these substitutions have been reported to
264 disrupt the binding interface between EPYC1 and *Cr*RBCS2 (He et al., 2020). Using
265 yeast-2-hybrid we confirmed that the interaction between the C-terminus of BST4 and
266 *Cr*RBCS2 was disrupted by these mutations (Fig. S3). When $BST4_{WR/EE}$-mCherry was
267 expressed with EPYC1-tGFP in $S2_{Cr}$, no enrichment of the mCherry signal was
268 observed in the Rubisco condensate (Fig. 4C, D). Thus, the RBMs of BST4 were
269 responsible for the enrichment of BST4 in the vicinity of the Rubisco condensate in
270 Arabidopsis.

271 However, when condensates were sedimented and analysed by immunoblotting,
272 BST4-mCherry was not detected in the condensate fraction (Fig. 4E). When leaf
273 samples were subjected to formaldehyde cross-linking prior to sedimentation of the
274 condensate, a small amount of BST4 was present in the condensate fraction. We
275 concluded that BST4 was not present in the condensate itself but preferentially
276 occupied the thylakoid membranes surrounding the *Cr*RBCS2-enriched condensate
277 (Atkinson et al., 2020), likely due to interactions with *Cr*RBCS2.

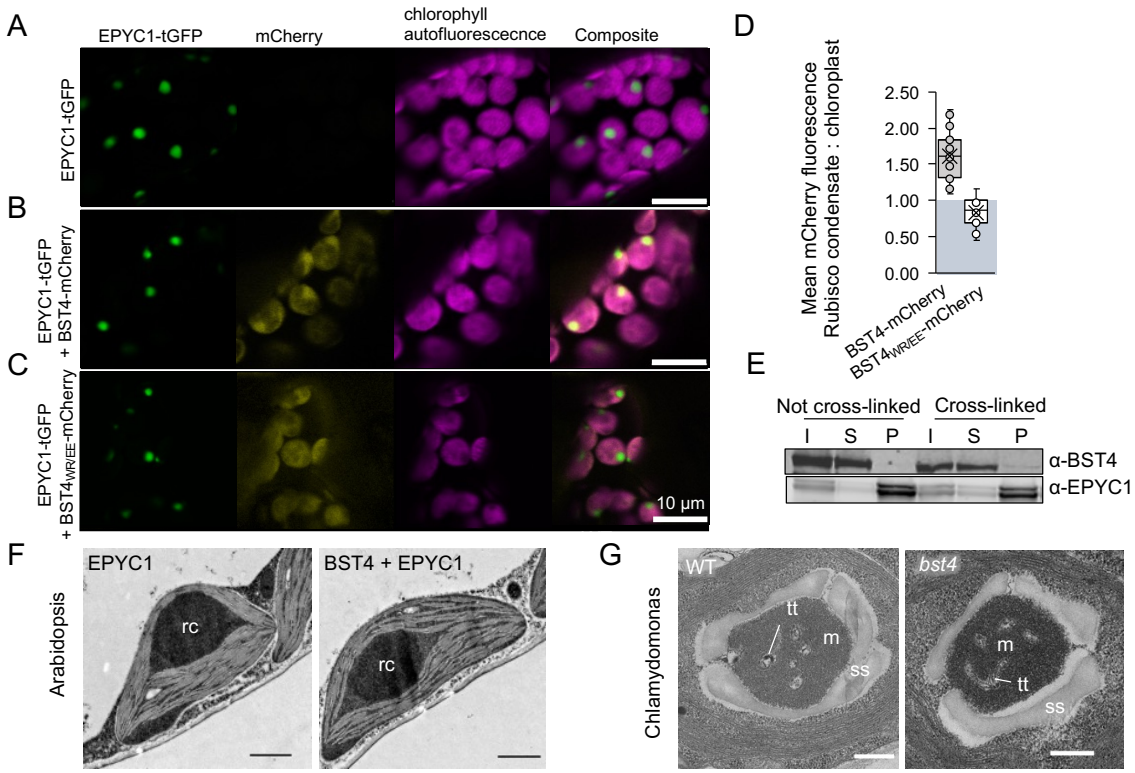

Figure 4. BST4 is not sufficient to enable the inclusion of thylakoid membranes in a Rubisco condensate in Arabidopsis and is not required for pyrenoid tubule inclusion in the Chlamydomonas pyrenoid. A. Confocal images showing EPYC1-tGFP in $S2_{Cr}$ Arabidopsis background. Scale bar is 10 µm. **B**. Confocal images showing BST4-mCherry co-expressed with EPYC1-tGFP in $S2_{Cr}$ Arabidopsis background. Scale bar is 10 µm. **C.** Confocal images showing BST4 with mutated RBMs ($BST4_{(WR/EE)}$) fused to mCherry co-expressed with EPYC1-tGFP in the $S2_{Cr}$ Arabidopsis background. **D.** Ratio of mean mCherry fluorescence associated with the Rubisco condensate compares do the rest of chloroplast when mCherry was fused to either BST4 or $BST4_{(WR/EE)}$ (n=22-23). **E.** Immunoblot of sedimented Rubisco condensates from $S2_{Cr}$ Arabidopsis expressing EPYC1-tGFP and BST4-mCherry. Abbreviations: I, input; S, supernatant; P, pellet. Rubisco condensates are enriched in the pelleted fraction. Cross-linked samples were prepared by vacuum infiltrating intact leaves with 1% (v/v) formaldehyde prior to sedimentation. **F**. Transmission electron micrograph of a chloroplast from $S2_{Cr}$ Arabidopsis expressing either EPYC1 alone or EPYC1-tGFP and BST4-mCherry. Rc is the Rubisco condensate. Scale bar is 1 µm. **G.** Transmission electron micrograph of pyrenoid from WT Chlamydomonas or *bst4* mutant. Abbreviations: tt, thylakoids tubules; p, pyrenoid; s, starch sheath. Scale bar is 1 µm.

Although BST4 partially co-localized with the Rubisco condensate, we found no evidence to suggest that that BST4 could facilitate the inclusion of thylakoid membranes. Confocal microscopy was not sufficient to determine if chlorophyll autofluorescence was in the proto-pyrenoids of $S2_{Cr}$ lines expressing BST4-mCherry and EPYC1-tGFP. However, transmission electron microscopy (TEM) revealed no visible indication of thylakoid membranes in the condensates, which were structurally similar to condensates in $S2_{Cr}$-EPYC1 lines lacking BST4 (Fig. 4F). Thus, BST4

302 appeared insufficient to enable thylakoid inclusion in the Rubisco condensate in
303 Arabidopsis.

304 **BST4 is not necessary for tubule formation in Chlamydomonas**

305 To investigate whether BST4 was necessary for normal formation of the thylakoid
306 tubule-structure in Chlamydomonas we compared the structure of pyrenoids of WT
307 and a BST4 knock-out line (*bst4*) (Fig. S3). TEM images showed that pyrenoids from
308 *bst4* were structurally comparable to the WT control, including the presence of
309 pyrenoid tubules (Fig. 4G). There were also no differences in pyrenoid size or shape
310 between the two lines when comparing pyrenoids from 40-50 cells from each genotype
311 (Fig. S4). As a result, we conclude that BST4 is not necessary for the pyrenoid tubule-
312 Rubisco matrix interface in Chlamydomonas. We speculate that BST4 may require a
313 pre-existing pyrenoid tubule network to be localized in the pyrenoid rather than driving
314 the inclusion of thylakoid membranes into the Rubisco matrix, or is redundant as a
315 tether protein.

316 **The C-terminus of BST4 is required for localisation to the pyrenoid tubules**

317 Meyer et al., 2020 previously demonstrated multiple copies of the BM are sufficient t
318 target proteins to the pyrenoid. In Fig. S2A we show that the BST4 RBMs are required
319 for RBCS interaction via yeast-2-hybrid and in Fig. 4B-D we show they are required
320 for enrichment with the proto-pyrenoid in Arabidopsis. To investigate the role of the
321 RBMs in BST4 localization in Chlamydomonas, we generated a truncated version of
322 BST4 (residues 1 to 386) that lacked the C-terminus containing the two RBMs
323 ($BST4_{\Delta C\text{-term}}$) and compared localisation with full-length BST4 expressed in WT and
324 the *bst4* mutant (Fig. 5 and Fig. S5). $BST4_{\Delta C\text{-term}}$-mScarlet expressed in the *bst4*
325 mutant line did not localize to the pyrenoid tubules but was found throughout the
326 thylakoid membrane (Fig. 5). This is consistent with our findings in Arabidopsis with
327 $BST4_{WR/EE}$ (Fig. 4C), demonstrating that localization of BST4 is driven via RBM-
328 Rubisco interaction. Thus, the C-terminus is necessary for BST4 localisation to the
329 pyrenoid tubules in the presence of the matrix.

330 When $BST4_{\Delta C\text{-term}}$-Venus was expressed in WT Chlamydomonas (i.e., that still
331 produced non-truncated BST4), we observed fluorescence throughout the thylakoids,
332 but with the majority of the signal still localized to the pyrenoid tubules (Fig. S5). We

333 conclude that BST4$_{\Delta C\text{-term}}$-Venus is recruited to the pyrenoid through an interaction
334 with the native full-length BST4, which is further evidence that BST4 oligomerizes.

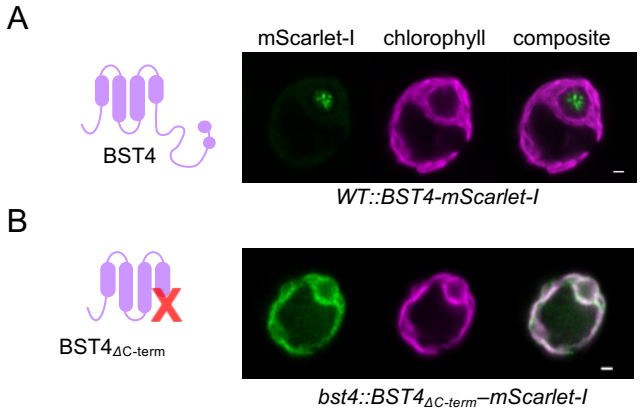

335

336 **Figure 5. C-terminus of BST4 is required for pyrenoid localization. A.** Confocal image of full length BST4-
337 mScarlet-I in WT **B**. Confocal image of BST4$_{\Delta C\text{-term}}$-mScarlet-I in *bst4*. Scale bars are 1 µm.

338 We next investigated whether BST4 localizes to the pyrenoid tubules, or whether
339 BST4 localizes to the tubules through an interaction with Rubisco. To do so, we utilized
340 a Chlamydomonas mutant generated by Genkov et al. (2010) that expresses *At*RBCS
341 but lacks both isoforms of *Cr*RBCS (*Crrbcs::AtRBCS*), and thus lacks a Rubisco matrix
342 as EPYC1 does not interact with *At*RBCS (Atkinson et al., 2019). *Crrbcs::AtRBCS*
343 retains reticulated thylakoid membranes at the canonical pyrenoid site, which are likely
344 the nascent pyrenoid tubule network (Caspari et al., 2017) (Fig. S6A). Caspari et al.
345 (2017) show large starch granules accumulating at the canonical pyrenoid site, which
346 we confirmed by expressing STA2-Venus as a starch marker (Mackinder et al., 2017)
347 in *Crrbcs::AtRBCS* (Fig. S6B). We expressed BST4-Venus in *Crrbcs::AtRBCS* and
348 found that BST4 localized to a punctum adjacent to the canonical pyrenoid site, which
349 we attribute to the nascent pyrenoid tubules (Fig. S6C). To confirm this, we also
350 expressed a known pyrenoid tubule marker protein, PsaF (Emrich-Mills et al., 2021)
351 in *Crrbcs::AtRBCS*, which showed a similar localisation pattern to that of BST4 (Fig.
352 S6D). This suggests there may be an additional Rubisco-binding independent
353 mechanism for localisation of BST4 as well as other proteins to the pyrenoid tubules.
354 Further investigation of the role of the whole C-terminal domain will be required to
355 understand the mode of BST4 pyrenoid tubule localisation.

356 **Chlamydomonas KO mutant *bst4* does not have a defective CCM but is under**
357 **oxidative stress**
358 To test whether BST4 has a role in the operation of the CCM, we measured the growth
359 of *bst4* compared to WT under various CO_2 conditions (Fig. 6). Semi-quantitative spot
360 assays indicated no reduction in growth under CO_2-limiting conditions (Fig. S7). The
361 liquid growth assay also demonstrated that *bst4* grew well in both CO_2 replete and
362 limiting conditions, 3% and 0.04%, respectively (Fig. 6A). The *bst4* mutant had a
363 slightly increased cell density compared to WT (Fig. 6A) in the 0.04% CO_2 treatment.
364 However, when comparing the calculated specific growth rates (μ h^{-1}) for both the
365 exponential growth phase (days 0-3, *bst4* 0.0402 ± 0.0003 μ h^{-1} and WT 0.0389 ±
366 0.0007 μ h^{-1}) or the full growth assay (days 0-5, *bst4* 0.0257 ± 0.0001 μ h^{-1} and WT
367 0.0241 ± 0.001 μ h^{-1}), there was no statistically significant increase in specific growth
368 rates between *bst4* and WT (two-tailed t-test, $p = 0.17$ and 0.20, respectively, $n = 3$,
369 full results Table S1). In combination, we concluded that BST4 is not an essential
370 component of the CCM and may therefore have a redundant or regulatory role. We
371 also included the complemented *bst4::BST4* and *bst4::BST4*$_{\Delta C\text{-}term}$*-mScarlet-I*
372 (hereafter *bst4::BST4*$_{\Delta C\text{-}term}$) lines in the spot and liquid growth assays. While all lines
373 grew well in the spot assay, in the liquid growth *bst4::BST4*$_{\Delta C\text{-}term}$ grew comparably to
374 WT and *bst4* whereas *bst4::BST4* exhibited a slightly reduced growth than the other
375 lines in both CO_2 conditions.

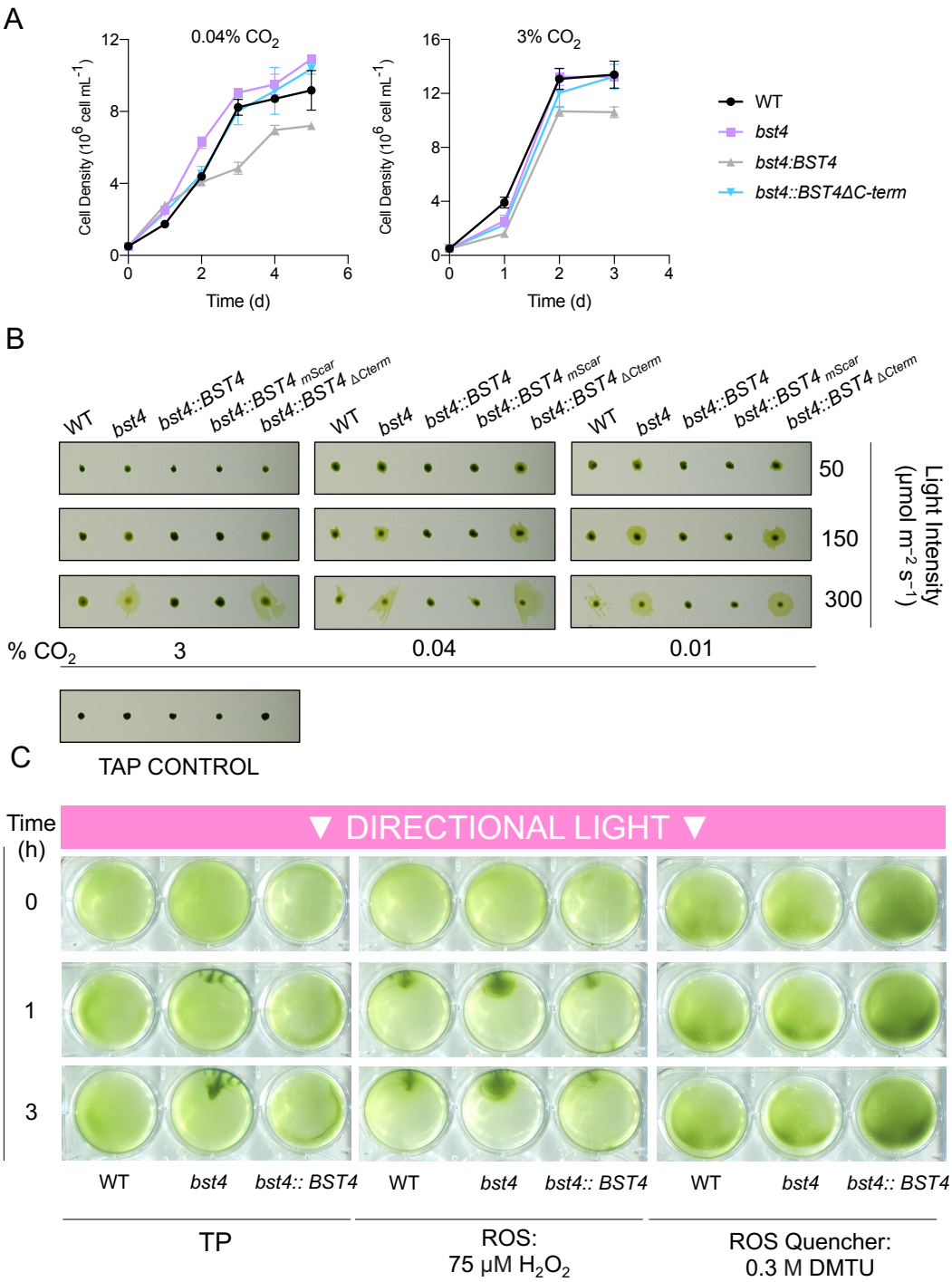

Figure 6. The *bst4* mutant does not have an impaired growth phenotype under CCM induced conditions but is associated with oxidative stress. A. *Chlamydomonas* strains were subjected to a liquid growth assay using pH 7.4 TP media that was bubbled with 0.04% CO_2 or 3% CO_2. Error bars are ± SEM, n=3. **B.** Dot assay of WT, *bst4,* complemented *bst4::BST4* and *bst4* complemented with C-terminal truncation of BST4 (*bst4::BST4*$_{\Delta C\text{-term}}$) on minimal TP agar at indicated light intensities and CO_2 concentrations. **C**. Phototaxis assay. Liquid cultures of Chlamydomonas cells were uniformly distributed on 0.8% (w/v) agar and directional light applied. Cell phototaxis was monitored by aerial photographs of wells at 0, 1, and 3 h. The assay was performed in the presence of 75 µM ROS hydrogen peroxide (H_2O_2) or 0.3 M ROS quencher N,N'-dimethylthiourea (DMTU).

One noticeable difference between *bst4* and WT lines from the growth assays conducted on solid media (Fig. 6B and S8) was that *bst4* cells had a distinct halo of

387 diffuse cells on the periphery of the colony. We used a range of CO_2 and light
388 conditions to investigate the diffuse colony phenotype (Fig. 6B) and found it was most
389 apparent under high light (300 µmol photons m^{-2} s^{-1}) and low or very low CO_2
390 conditions (0.04% CO_2, 0.01% CO_2, respectively). WT, *bst4::BST4* and *bst4::BST4-*
391 *mScarlet-I* complemented lines had little or no diffusivity, although WT did display a
392 slightly diffuse colony phenotype at 300 µmol photons m^{-2} s^{-1}. Interestingly, $BST4_{\Delta C-}$
393 $_{term}$-mScarlet-I was unable to rescue the diffuse colony phenotype suggesting that
394 either the presence of the C-terminus or localization to the tubules is essential for the
395 function of BST4.

396 The diffuse colony phenotype was most apparent under high light (300 µmol photons
397 m^{-2} s^{-1}) and exacerbated by low CO_2 (0.01 and 0.04%), at medium light (150 µmol
398 photons m^{-2} s^{-1}) which are conditions where carbon fixation can be limiting and
399 therefore, the light dependent and light independent reactions of photosynthesis are
400 unbalanced. This imbalance can result in the release of Reactive Oxygen Species
401 (ROS) (Erickson et al., 2015). It has previously been shown that cells exposed to ROS
402 have altered phototactic responses to light (Wakabayashi et al., 2011), which may
403 explain the diffuse colony phenotype we observed. To test this hypothesis, we
404 exposed Chlamydomonas cells in liquid culture to directional light (150 µmol photons
405 m^{-2} s^{-1}) (Fig. 6C). In this assay, *bst4* cells displayed strong positive phototaxis,
406 whereas WT and complemented *bst4::BST4* lines displayed negative phototaxis,
407 indicating that *bst4* cells may be experiencing oxidative stress.

408 To confirm that the phototactic response of *bst4* was due to oxidative stress, we
409 recorded the direction of phototaxis in cells exposed to either ROS or a ROS quencher.
410 In the presence of the ROS quencher N,N'-dimethylthiourea (0.3 M DMTU), *bst4*
411 positive phototaxis was disrupted, resulting in a negative response to directional light
412 (Fig. 6C). When the ROS H_2O_2 (75 µM) was added, WT, *bst4::BST4* and *bst4*
413 displayed positive phototaxis (Fig. 6C). Together, our data indicates that the direction
414 of phototaxis in *bst4* is due to the degree of oxidative stress.

415 ROS generation occurs under excess light which can be caused by either high light
416 conditions or limited CO_2 fixation due to an impaired CCM or low CO_2 availability
417 (Santhanagopalan et al., 2021; Choi et al., 2022). As *bst4* can maintain similar growth

418 to WT under low CO_2 conditions, we hypothesized that CO_2 fixation is not limiting in
419 this case. Rather, the absence of BST4 may disrupt regulation of the light reactions.

420 ***BST4* is associated with regulation of the lumenal pH in Chlamydomonas.**
421 To assess the impact of BST4 on the light reactions, we measured photosynthetic
422 parameters of WT, *bst4* and *bst4* complemented with either full length *BST4* or
423 $BST4_{\Delta C\text{-}term}$. Chlorophyll and carotenoid levels were slightly lower in *bst4*, however this
424 was not significantly different. Complementation with BST4 recovered chlorophyll and
425 carotenoid levels to a higher level than WT whilst in $bst4::BST4_{\Delta C\text{-}term}$ lines levels were
426 comparable to the *bst4* mutant (Fig. S9A).

427 Next, we measured the slow kinetics of chlorophyll fluorescence upon transition from
428 dark to high light to determine the impact of BST4 on the distribution of absorbed light
429 between non-photochemical quenching (NPQ) and electron transport through
430 photosystem II (Y(II)) (Fig. 7). F_v/F_m was slightly higher in *bst4, bst4::BST4* and
431 $bst4::BST4_{\Delta C\text{-}term}$ compared to WT (Fig. 7A). NPQ was induced faster and reached a
432 significantly higher steady state in *bst4* than in WT (Fig. 7B). In contrast, *bst4::BST4*
433 had WT-like NPQ. $bst4::BST4_{\Delta C\text{-}term}$ had an intermediate phenotype indicating
434 incomplete rescue of the high NPQ phenotype via $BST4_{\Delta C\text{-}term}$. No differences in Y(II)
435 were observed during the light phase (Fig. 7C). However, in the subsequent dark
436 phase, Y(II) in *bst4* recovered faster in line with the higher F_v/F_m (Fig. 7C).

437 The increase in NPQ suggested that BST4 influences the reactions occurring in the
438 thylakoid membrane. A higher steady-state NPQ indicates that the *bst4* cells
439 experience high light stress and respond by accelerating photoprotective excess light
440 dissipation to maintain optimal electron transport. This observation aligns with
441 increased ROS production observed in *bst4* (Fig. 6C), which would result in elevated
442 NPQ to compensate for the increase in oxidative stress. In the case of $bst4::BST4_{\Delta C\text{-}}$
443 $_{term}$, it is possible that the truncation directly affects BST4 activity. Alternatively, the
444 mis-localization of BST4 activity throughout the thylakoid membranes, instead of solely
445 localized to the thylakoid tubules, results in the disruption of optimal electron transport
446 and the need for increased photoprotection.

447 NPQ is induced in response to a drop in lumenal pH, a process that is mediated by
448 the quencher protein LHCSR3. Thylakoid ion channels can influence NPQ through

449 altering the partitioning of the proton motive force (PMF) into pH gradient (ΔpH) and
450 electrical gradient (ΔΨ). To investigate whether BST4 was altering lumenal pH we
451 measured the slow decay kinetics of electrochromic shift (ECS), which allows the
452 determination of PMF partitioning. WT and *bst4::BST4* displayed similar standard
453 kinetics. However, both *bst4* and *bst4::BST4*$_{\Delta C\text{-}term}$ had abnormal kinetics and did not
454 reach steady state (Fig. S8A, B). Therefore, we could not derive PMF partitioning for
455 all the genotypes. The abnormal ECS kinetics in *bst4* and *bst4::BST4*$_{\Delta C\text{-}term}$ may
456 indicate altered proton-related processes, such as over acidification of the thylakoid
457 lumen. We also measured the accumulation of protein LHCSR3 after exposing cells
458 to 150 μmol m^{-2} s^{-1} for 3 h and found that *bst4* accumulated more LHCSR3 as
459 compared to WT (Fig. 7G, H). In the complemented lines, *bst4::BST4* accumulated
460 similar levels to WT and *bst4::BST4*$_{\Delta C\text{-}term}$ accumulated less. The increased NPQ
461 observed in *bst4* may therefore be due to a combination of both upregulation of
462 LHCSR3 expression and altered lumenal pH.

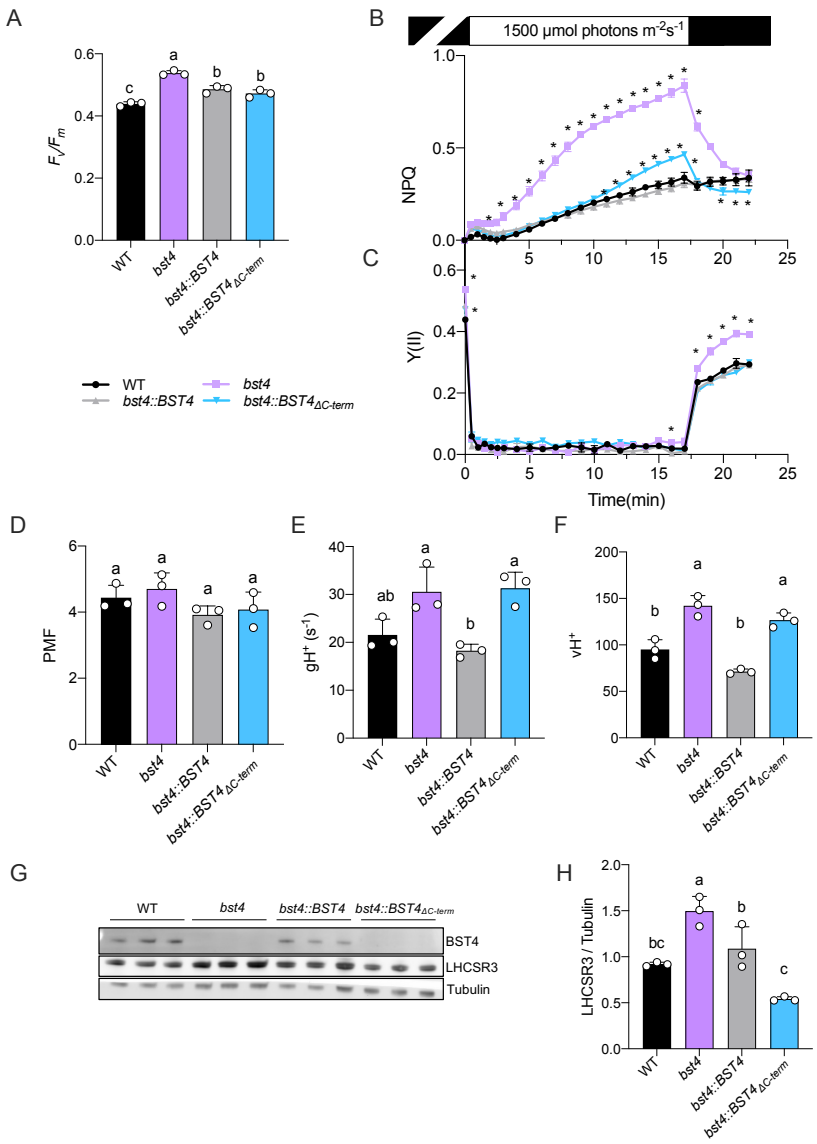

463

464 **Figure 7. Chlamydomonas *bst4* mutant has an enhanced NPQ and ATP synthase activity under limiting Ci**
465 **conditions.** Wild type (WT) and mutants were grown on TAP medium at 20 µmol photons m^{-2} s^{-1}, resuspended in
466 TP at 30 µg Chl ml^{-1} and exposed for 3 h to light at 150 µmol photons m^{-2} s^{-1}. The cells were dark adapted for 1 h
467 before the measurements. **A.** Maximum quantum yield of photosystem II. **B.** Dynamics of photosynthesis on
468 transition from dark to high light. Kinetics for induction of chlorophyll fluorescence were recorded during 17 min of
469 illumination at 1500 µmol photons m^{-2} s^{-1} followed by 5 min in darkness. Non-photochemical quenching (NPQ)
470 and **C.** Photosystem II quantum yield (Y(II)). **D to F.** ECS decay kinetics were performed on cells pre-exposed for
471 10 min to high light and the **D.** total PMF, **E.** g_H^+, and **F.** total H^+ flux (v_H^+) were determined as described in Methods.
472 Data are the means ± SEM (n=3 replicates). Different letters indicate statistically significant difference among the
473 genotypes (one-way ANOVA test, followed by Turkey's post hoc test, $P < 0.05$). Statistical analysis was performed
474 separately for measurements made with and without HCO_3^- (black and green letters, respectively). **G.** Immunoblot
475 of NPQ protein LHCSR3 in each genotype compared to tubulin after exposure of cells to 3 h 150 µmol photons m^{-2}
476 s^{-1} in TP. **H.** Fluorescence of LHCSR3 protein band normalized to α-tubulin. Data are the means ± SEM (n=3
477 replicates). Different letters indicate statistically significant difference among the genotypes (one-way ANOVA test,
478 followed by Turkey's post hoc test, $P < 0.05$).

479 To further explore the proton related processes, we recorded fast decay ECS kinetics
480 which allows for the determination of the total PMF size, as well as H^+ conductivity of
481 ATP synthase (g_{H^+}) (Fig. S9E). The PMF after 10 min of illumination did not
482 significantly differ among any of the genotypes (Fig. 7D). At the same timepoint, the
483 g_{H^+} was significantly higher in *bst4* and *bst4::BST4$_{\Delta C\text{-}term}$* than in WT and *bst4::BST4*
484 (Fig. 7E). We also calculated the total proton flux (v_{H^+}), which showed a similar trend
485 although v_{H^+} was also significantly lower in *bst4::BST4,* compared to WT (Fig. 7F).
486 Based on the proton flux data, we postulate that more ATP is produced in *bst4* and
487 *bst4::BST4$_{\Delta C\text{-}term}$* and less in *bst4::BST4* and WT. In the *bst4* mutant, H^+ in the lumen
488 are likely in excess and are used in H^+-dependent processes such as NPQ and ATP
489 synthesis.

490 We next proposed that BST4 might be an anion channel involved in regulating the pH
491 of the thylakoid lumen. To determine what BST4 may be permeable to, we expressed
492 BST4 in Xenopus oocytes and measured currents in the presence of different anions
493 (Fig. S9A). Bestrophins are typically permeable to Cl^- and HCO_3^- but no currents for
494 BST4 were detected in the presence of 100 mM KCl or 100 mM $NaHCO_3$. As some
495 bestrophins are autoinhibited by their C-terminus (Qu et al., 2006), we also tested two
496 C-terminal truncations of BST4 (0-386 and 0-591), but no currents were detected.
497 Another possibility is that BST4 is permeable to organic ions, similarly to *Hs*Best1,
498 which has been shown to be permeable to **γ**-aminobutyric acid (GABA) (Lee et al.,
499 2010) and glutamate (Woo et al., 2012), as well as Cl^- and HCO_3^- anions. Fei et al.
500 (2022) proposed a model whereby RuBP acts as proton carrier to increase H^+
501 concentration in the pyrenoid tubules. It is possible that BST4 is the channel that
502 facilitates RuBP translocation in the tubules in this model. To test this hypothesis, we
503 used small molecule analogues K-PEP and K-Gluconate but no currents were
504 detected for these either (Fig. S9A). Therefore, we were unable to draw conclusions
505 as to what BST4 is permeable to. BST4 may require certain conditions to be open that
506 are not met in the oocyte system, such as post-translational modifications, a specific
507 pH or an interaction partner. BST4 was found to be phosphorylated and had an
508 oxidized methionine residue in its C-terminus (Bergner et al., 2015). Methionine
509 oxidation can serve as channel-regulating post translational modification (Ciorba et
510 al., 1999), which would fit with the role that BST4 appears to have in preventing
511 oxidative stress.

512 **BST4 has no impact on growth in Arabidopsis $S2_{Cr}$ line**

513 Although the permeability is undefined, if BST4 is a functional anion channel, it is
514 possible that its presence in plant thylakoid membranes might have an effect. We
515 generated three independent BST4 no tag lines in the $S2_{Cr}$ background and used them
516 to assess the impact of BST4 on Arabidopsis physiology (Fig. S10A). We found there
517 was no difference in growth between plant expressing BST4 and their azygous
518 segregants, as determined by the rosette area (Fig. S10B). We also found that BST4
519 expressing plants tended to have slightly lower F_v/F_m as compared to azygous
520 segregants and the parent line, although this was not significant (Fig. S11C). Further
521 measurements were made for lines 2 and 3 on the kinetics of NPQ, Y(II) and for PMF
522 size and partitioning but no consistent differences were observed (Fig. S11).

523 **Proposed model for the role of BST4 in the Chlamydomonas pyrenoid**

524 Based on these findings, we speculate that BST4 may have a regulatory role in the
525 CCM through its function as a bestrophin channel. We propose two possible models
526 to explain our data. The first model is that BST4 is functioning as an anion channel to
527 import anions from the pyrenoid into the thylakoid lumen. This would counterbalance
528 the charge of protons in the tubules, possibly contributing to pH regulation or
529 maintaining a high flux of protons towards the pyrenoid to power the CCM (Figure 8).
530 The absence of BST4 would cause disruption of lumen pH or cause a drop in CCM
531 efficiency that causes stress under high light and low CO_2. The second model is that
532 BST4 is part of a HCO_3^- recovery system to takes up HCO_3^- from within the pyrenoid,
533 allowing HCO_3^- to be transported back into the tubules where it can be dehydrated to
534 CO_2 and thus available to be fixed by Rubisco. In this scenario, the absence of BST4
535 would lead to a slight reduction in CCM operation efficiency, perhaps not sufficient to
536 cause a growth penalty but enough to cause a build-up of protons in the tubule lumen
537 and alter the homeostasis of the light reactions. Further work is required to elucidate
538 the function of BST4, primarily, determining what species BST4 is permeable to, any
539 modes of channel regulation and possible interaction partners.

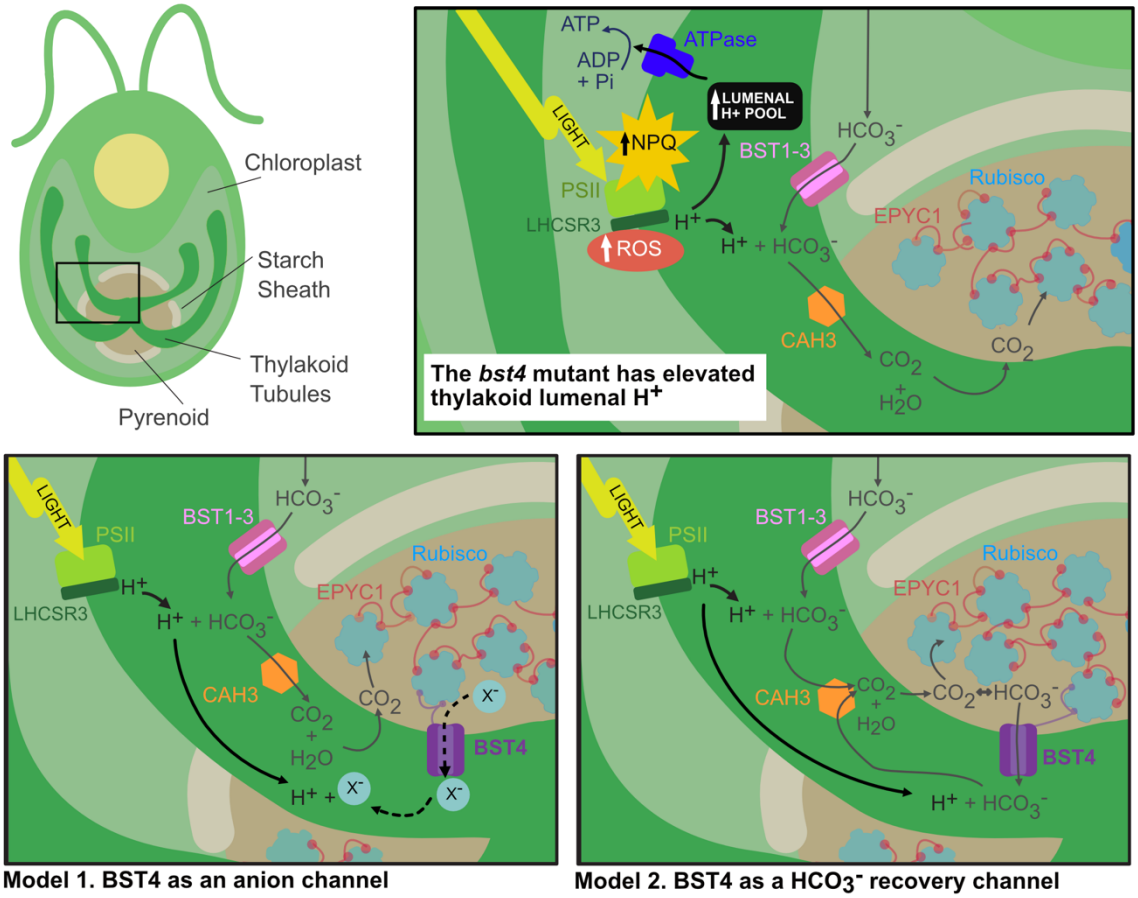

Figure 8. The role of BST4 in light and CO_2 limiting conditions. The data presented here show that in the *bst4* knock-out line there is increased ROS production. There is also likely an over acidified thylakoid lumen, which causes elevated NPQ and increased ATP generated through ATP Synthase activity. We suggest that BST4 functions as a thylakoid membrane channel, which plays a role in balancing the light reactions with carbon fixation while the CCM is active. In this role, we propose BST4 is a channel that facilitates the transport of anions from the pyrenoid matrix into the thylakoid lumen whereby they act as a sink for available protons (Model 1). It is possible that BST4 is specifically a HCO_3^- channel (Model 2) that facilitates the recovery of HCO_3^- from the pyrenoid matrix. This would subsequently enable CAH3 to catalyse the dehydration of HCO_3^- into CO_2, which is then able to diffuse back into the pyrenoid and be fixed by Rubisco.

MATERIALS AND METHODS

Phylogenetic Analysis

Sequences for phylogenetic analysis were compiled by blasting of BST4 (Cre06.g261750) in the NCBI database (Sayer et al 2022) and the manual addition of other well characterized bestrophin proteins including BEST1 *Homo sapiens* (XP_011543531.1), KpBEST *Klebsiella aerogenes* (WP_049046555.1), VCCN1 from *Arabidopsis thaliana* (Q9M2D2) and BST1-3 *Chlamydomonas reinhardtii* (Cre16.g662600, Cre16.g663400 and Cre16.g663450). Sequences were aligned using MAFFT (Katoh and Standley, 2013) visually inspected and manually trimmed (specified). Finalized alignments were run through IQTREE webserver (Minh et al.,

560 2020) to identify the most appropriate substitution model. Maximum likelihood trees
561 were then generated in Geneious v11 using the PhyML 3.0 (Guindon et al., 2010)
562 plugin with a LG substitution model (Le and Gascuel, 2008) with Gamma distribution
563 (4 categories) and 500 bootstrap iterations. Full alignments are found in Fig. S12.

564 **Alphafold structure prediction**

565 Five chains of BST4 were submitted to Alphafold Multimer v2 with default settings.
566 The top ranked model of five was used for figure generation.

567 **Generation of plasmids**

568 The plasmids for BST4 mutant complementation in *Chlamydomonas* were prepared
569 using a recombineering method described previously (Emrich-Mills et al., 2021). BST4
570 is expressed under native promotor with either without a tag or with an mScarlet-I C-
571 terminal tag, and a hygromycin AphVII selection marker.

572 Plasmids for plant expression were generated using the MoClo system (Engler et al.,
573 2014). For visualisation, BST4 was combined with 35S promoter (pICH51277),
574 mNeonGreen C-terminal tag (pICSL50015), HSP terminator and acceptor plasmid
575 (pICH47732) and a pFAST-R section cassette used for selection. For all other
576 experiments a no-tag BST4 construct was generated with the 35S protomer and HSP
577 terminator parts and a Kanamycin resistance cassette was used for selection.

578 Plasmids for Xenopus expression were generated by using the Gateway system by
579 cloning the coding sequence for BST4 into pGT vector (Grefen et al., 2010) was
580 amplified with Gateway adaptor sequences from a synthesized as g-block (IDT) with
581 the PredAlgo (Tardif et al., 2012) predicted transit peptide removed from the N-
582 terminal (sequence begins R35), any subsequent mutations were made via PCR.

583 **Arabidopsis transformation**

584 Arabidopsis was transformed by floral dip as previously described in (Atkinson et al.,
585 2016). BST4-mNeon primary transformants were screened for transgene insertion by
586 seed fluorescence from pFAST-R and BST4 expression was confirmed by checking
587 for mNeon fluorescence and by immunoblot. BST4 no tag primary transformants were
588 screened using kanamycin resistance and immunoblot. Zygosity was checked via
589 seed fluorescence from pFAST-R or kanamycin resistance.

590 **Chlamydomonas cell culture conditions and strain details**

591 *Chlamydomonas reinhardtii* cultures were maintained as previously described (Ma et
592 al., 2011). Tris-Acetate-Phosphate (TAP) and minimal (TP) media (acetate free) were
593 prepared according to Sueoka (1960). TAP and TP agar plates for growth were made
594 by adding 1.5% (w/v) agar. CMJ030 (CC-4533; *cw15, mt⁻)* and *bst4* (BST4 knock-out
595 LMJ.RY0402.159478) were obtained from the CLiP collection at the *Chlamydomonas*
596 culture collection (Zhang et al., 2014; Li et al., 2015). The insertion of the CIB1 cassette
597 in *BST4* was confirmed by PCR amplifying the insertion locus from genomic DNA (Fig.
598 S3A) using loci specific primers (forward GAGCTTCGTGGATGGATGTT and reverse
599 GTATGAAGGTCACCGCCTGT) in parallel with a control locus (forward
600 ATGCTTCTCTGCATCCGTCT and reverse ATGTTTTACGTCCAGTCCGC). The *bst4*
601 knock-out was complemented with *BST4* constructs described herein. All
602 complemented lines were validated by western blotting of BST4 and specified epitope
603 tags, described below (Fig. S3B-E).

604 **Chlamydomonas transformation**

605 For each Chlamydomonas transformation, 28 ng kbp^{-1} of plasmid was linearized by
606 restriction digest. Cells were grown to 2-4 x 10^6 cell mL^{-1}, harvested by centrifugation
607 at 1000 xg for 10 min and resuspended in TAP with 40 mM Sucrose at a concentration
608 of 2 × 10^8 cells mL^{-1}. Linearized plasmid was mixed with 250 µL of cells at 15°C in a
609 0.4 cm gap electroporation cuvette and transformed immediately by electroporation
610 using a Gene Pulser II (Bio-Rad) set to 800V and 25 µF. Cells were recovered
611 overnight in TAP Sucrose while shaking gently (140 rpm) in the dark. Transformed cell
612 were subsequently subjected to selection by growth on TAP agar plates with
613 paromomycin (20 µg mL^{-1}) or hygromycin (25 µg mL^{-1}) which were kept in low light
614 (5–10 µmol photons m^{-2} s^{-1}) until screening positive transformants.

615 **Chlamydomonas Growth Assays**

616 Spot Tests: Cells were grown heterotrophically in TAP media. Once cultures reached
617 2-4 x 10^6 cell mL^{-1}, 1 x 10^6 cells were harvested by centrifugation at 1000 xg for 10
618 min. Cell were washed and resuspended at a concentration of 1 x 10^6 cell ml^{-1} in TP
619 media. Liquid cultures were spotted onto TP agar (1.5%) in 1000, 100 and 10 cell
620 spots at a range of pHs (specified). The plates were incubated in 3, 0.04 and 0.01%
621 CO_2 and illuminated under constant light at 400 µmol photons m^{-2} s^{-1}. Growth was
622 monitored for up to 10 days.

623 Liquid Growth: Cells were grown heterotrophically in TAP media. Once cultures
624 reached 2-4 x 10^6 cell mL^{-1}, cells were harvested by centrifugation at 1000 xg and
625 resuspended at a starting concentration of 1 x 10^5 cell ml^{-1} in TP media pH 7.4.
626 Cultures were incubated in a CellDEG HDC 22.10 culture platform (CellDeg GMBH,
627 Berlin) bubbled with 0.04 and 3% CO_2, illuminated at 150 µmol photons m^{-2} s^{-1} and
628 consistently stirred at 180 rpm. Cell density and optical destiny (750 nm)
629 measurements were taken daily for up to 10 days. Specific growth rates (SGR) per h
630 were calculated using the following formula, $ln(N_2/N_1)/t$ whereby N = cell density.

631 Dot tests: Cultures were grown in a 96 format on agar plates and replicated by a Rotor+
632 (Singer Instruments) high throughput replication robot. The cultures were stamped
633 onto pH 7.8 TP agar plates, incubated in 3, 0.04 and 0.01% CO_2 and illuminated under
634 constant light at a range of intensities (specified). Growth was monitored for up to 10
635 days.

636 **Phototaxis Assays**

637 Chlamydomonas cells were grown heterotrophically in TAP media until they reached
638 2-4 x 10^6 cell mL^{-1} and harvested by centrifugation at 1000 xg for 10 min. Pelleted cells
639 were either re-suspended in TP media or, for ROS manipulation assays, a phototaxis
640 buffer described previously by Ueki et al. (2016) (5 mM Hepes pH 7.4, 0.2 mM EGTA,
641 1 mM KCl, and 0.3 mM $CaCl_2$). The assays took place in 12-well dishes with a thin
642 layer of TP agar (0.8%) on the well bottom and approximately 1.5 x 10^7 cells in 400 µL
643 of homogenous suspension laid on top. The dishes were illuminated from one direction
644 with 150 µmol photons m^{-2} s^{-1} illumination for up to 3 h. Plates were imaged using a
645 Flatbed Scanner at specified intervals.

646 **Growth of Arabidopsis**

647 Arabidopsis seeds were sown on moist F2+S soil and stratified in the dark at 4℃ for 2
648 days. For growth experiments seeds were grown in a Percival SE-41AR3cLED
649 chamber (CLF PlantClimatics GmbH, Wertingen, Germany) equipped with cool white
650 LED lights under 12 h light (175-180 µmol photons m^{-2} s^{-1})/12 h dark cycles at 21°C,
651 respectively and 70% relative humidity.

652 **Chlamydomonas Confocal Microscopy**

653 Transgenic fluorescent strains were initially grown heterotrophically in TAP media until
654 reaching 2 – 4 $\times 10^6$ cells mL^{-1} and resuspended in TP media overnight prior to
655 imaging. Cells were mounted on 8-well chamber slides and overlayed with 1.5% low
656 melting point agarose made with TP-medium. Images were collected on a LSM880
657 (Zeiss) equipped with an Airyscan module using a 63× objective. Laser excitation and
658 Emission setting for each channel used are set as below: Venus (Excitation: 514 nm;
659 Emission 525 – 500 nm); mScarlet-I (Excitation: 561 nm; Emission 570 – 620 nm);
660 Chlorophyll (Excitation: 633 nm; Emission 670 – 700 nm).

661 **Slimfield microscopy**

662 Chlamydomonas lines *bst4::BST4-mScarlet-I* and the unlabelled control line *bst4* were
663 prepared overnight in TP media. Each was harvested and spotted onto a slide-
664 mounted agar pad (GeneFrames, ThermoFisher), consisting of TP media with 1.5%
665 low melting point agarose. Fluorescence imaging with single-molecule sensitivity was
666 performed using a custom Slimfield microscope (Syeda et al., 2019). The setup used
667 a high-magnification objective (NA 1.49 Apo TIRF 100× oil immersion, Nikon) and the
668 detector was a Prime95B sCMOS camera (Teledyne Photometrics) operating in 12-
669 bit 'sensitivity' gain at a high total magnification of 53 nm/pixel. The samples were
670 illuminated either in brightfield, or for Slimfield fluorescence in camera-triggered
671 frames by a collimated 561 nm wavelength, Gaussian mode OPSL laser (Coherent,
672 Obis LS) at a peak intensity of 5 kW/cm^2 at the sample plane. This beam was tilted
673 into a HILO configuration (Payne-Dwyer and Leake, 2022) to reduce out-of-focus
674 excitation while retaining quantitative molecular sensitivity. The fluorescence image
675 was split into two parallel channels comprising emission bandpass filters (Semrock
676 BrightLine®): one with a 585/15 emission filter (central wavelength/spectral bandwidth
677 in nm) optimized to isolate the mScarlet-I signal, and a second with a 525/25 emission
678 filter, used only to indicate autofluorescence background. The total length of each
679 acquisition sequence was ~5 s; sufficient to observe the full course of mScarlet-I
680 photobleaching, from the initial unbleached state to single-molecule blinking, while
681 also rapid enough (10 ms exposure/frame at 180 frames/s) to capture the motion of
682 individual molecular assemblies.

683 **Single particle tracking and molecular counting**

684 Slimfield image sequences were segmented manually in ImageJ to include only the
685 pyrenoids in downstream analysis. The centroid positions of fluorescent tracks were
686 identified from local intensity maxima in each frame using ADEMScode software in
687 MATLAB (Wollman et al., 2022). The summed intensity of each candidate track was
688 calculated in each frame by adding all pixel values within 5 pixels of the centroid, then
689 subtracting the local background averaged between 5-8 pixels from the centroid.
690 Candidates with a summed intensity <0.4× the standard deviation in the background
691 region were discarded.

692 Fluorescent proteins are known to exhibit a characteristic integrated intensity per
693 molecule under stable Slimfield imaging conditions and within the quasi-uniformly
694 illuminated area within half the beam waist (Shepherd et al., 2021). After sufficient
695 photobleaching of mScarlet-I in the Slimfield image sequences, only step-like blinking
696 was observed at the end of each track. The modal integrated intensity of these steps
697 was used to estimate this characteristic single molecule brightness, equivalent to 56
698 ± 9 photoelectrons per frame per molecule.

699 At the start of each track, we obtained an initial integrated intensity (independent of
700 photobleaching) by linearly extrapolating the summed intensity backwards over the
701 first 4 frames of the exposure. This initial intensity was then divided by the
702 characteristic brightness of a single mScarlet-I to estimate the number of molecules,
703 or stoichiometry, in that track. This estimate was precise enough to detect
704 stoichiometry steps of up to 12 tagged molecules without ambiguity.

705 Stoichiometry distributions may exhibit peaks which are separated by a characteristic
706 interval. The smallest consistent interval between peaks can be used to infer the size
707 of a physical repeat unit or 'periodicity' within assemblies (Hunter et al., 2022; Payne-
708 Dwyer et al., 2022). A kernel width of 0.7 molecules was chosen to generate the
709 stoichiometry distribution (Fig. 2F), reflecting the background standard deviation.
710 Peaks were pinpointed using MATLAB's *findpeaks*.

711 The intervals between all peaks for each acquisition were aggregated across the
712 pyrenoid population, weighted by inverse square-root distance (thereby accounting for
713 shot-noise in broader intervals). A second distribution (Fig. 2G) was then generated
714 from this weighted population of intervals. The kernel width in this estimate was 0.7

715 molecules multiplied by the square root of the mean stoichiometry divided by the root
716 number of intervals (thereby accounting for shot-noise in intervals between peaks of
717 higher stoichiometry). The periodicity was then reported as the mode of this
718 distribution and its 95% confidence interval.

719 **Arabidopsis Confocal microscopy**

720 Small sections of 3–4-week-old leaf tissue (~5-10 mm^2) were adhered to slides using
721 double-sided tape with basal side up. A x40 water immersion objective lens was used.
722 Samples were excited by 488 nm at 1% laser power, chlorophyll autofluorescence was
723 collected at 680 – 750 nm and mNeonGreen fluorescence at 503–532 nm. For dual
724 tagged lines, we used sequential acquisition to minimise bleed-through. mCherry was
725 excited using the 542 nm laser and emission collected at 601-620 nm and mNeon as
726 before. Images were acquired using the SP8 Confocal system and Leica LAS AF
727 software (http://www.leica-microsystems.com/). Figures were prepared using ImageJ
728 (http://fiji.sc/Fiji).

729 **Immunoblot detection**

730 Two leaf disks (6 mm diameter) were harvested and immediately frozen in liquid
731 nitrogen. Two steel balls (3 mm) were added and tissue was homogenized using a
732 tissue-lyser twice for 30 Hz for 30 s. A four times volume of cold extraction buffer (20
733 mM Tris-HCl pH = 7.5, 5 mM $MgCl_2$, 300 mM NaCl, 5 mM DTT, 1% (v/v) Triton X-100,
734 1 x Protease inhibitor (Roche)) was added and samples vortexed for 30 s. Samples
735 were solubilized on ice for 5 mins and then centrifuged at 5000 x g for 5 min at 4℃.
736 17.5 µL of supernatant was used to make up 1x LDS and 100 uM DTT. 20 µL was
737 loaded on a Novex™ 4-12% Bis-Tris Mini Gel, (Thermo Fisher, Catalogue number:
738 NP0322BOX). The gel was run at 150 V for 60 minutes. Proteins were transferred to
739 a nitrocellulose membrane using an iBlot 2, programme 0. The membrane was probed
740 with primary antibody in 5% milk in 1 x TBST at the following dilutions: BST4 (1:1000;
741 generated for this study, peptide from C-terminus: SDTELSEANRPRTRPDWRN)
742 (YenZym, Antibodies LLC, USA), AtpB (1:2000; Agrisera:AS05085), RbcL (1:1000;
743 kind gift from Griffiths lab), CP43 (1:3000; Agrisera: AS111787), PsaB (1:1000;
744 Agrisera: AS10695), PsbO (1:2000; Agrisera:AS06142-33). Secondary antibody (goat
745 α-rabbit IR-800; Li-COR: 925-32211). Membrane was imaged using the Li-COR
746 Odyssey CLx scanner.

747 In order to quantify BST4 protein in Chlamydomonas lines, cells were grown in TP
748 media at ambient CO_2 until reaching 2-4 x 10^6 cells mL^{-1}. Cells were harvested by
749 centrifugation at 1000 x g for 10 mins, normalized to Chl content and resuspended in
750 the extraction buffer described above. Samples were freeze-thawed three times and
751 spun at 20, 000 x g for 20 min at 4℃. Protein extractions containing 5 µg of Chl with 1
752 x SDS loading buffer were boiled at 100℃ for 5 min and loaded onto a 4-20%
753 polyacrylamide gel (Mini Protean TGX, Biorad Laboratories). Proteins were
754 transferred to a PVDF-FL membrane on a Bio-rad semidry blotting system. BST4
755 primary antibody was used as described above alongside alpha-tubulin primary
756 antibody raised in mouse (Agrisera), as a loading control. Anti-rabbit and anti-mouse
757 fluorescent secondary antibodies, Invitrogen AlexaFluor 488 and 555 respectively,
758 were used at a 1:20 000 dilution. Immunoblots were imaged using an Amersham
759 typhoon 5 scanner with 488 and 535 excitation lasers and Cy2 and Cy3 emission
760 filters. BST4 band fluorescent intensity was quantified using FIJI (Image J) (Schindelin
761 et al., 2012) and normalized to alpha-tubulin loading control. All Chlamydomonas lines
762 for quantification were extracted and analysed in triplicate. For LHCSR3 protein
763 quantification, cells were seeded at 0.1 OD_{750} in TAP media for 4 days and then
764 switched to TP media at a concentration of 30 µg Chl ml^{-1} and exposed to 150 µmol
765 photons m^{-2} s^{-1} for 3 h. Protein was extracted according to Burlacot et al. 2022 and
766 separated by SDS-PAGE as described for BST4 immunoblots.

767 Oocytes for expression of BST4 were collected after recording and prepared for
768 western blot as described in Lefoulon et al., 2018. The BST4 primary antibody was
769 used as described above and the secondary antibody used was horseradish
770 peroxidase-coupled goat, anti-rabbit (dilution 1:10000 Abcam). Proteins were detected
771 with ECL Advance kit (GE Healthcare,Poole UK).

772 **Blue-Native PAGE**

773 A crude thylakoid enrichment was performed according to (Aro et al., 2004). Thylakoid
774 membranes were solubilized in 0.5% DDM, 1x NativePAGE buffer (Thermo: BN2003),
775 1x cOmplete protease inhibitor tab (Roche;10x stock made by dissolving 1 tablet in 1
776 mL dH_2O) for at a concentration of 0.8 µg Chl/µl for 15 min on ice. Unsolubilized
777 material was removed by two rounds of centrifugation at 17,000 xg at 4°C for 15 min.
778 19.5 µL of supernatant was combined with 0.5 µL of Coomassie additive and loaded

779 immediately onto a 4-16% Bis-tris gel (Thermo: BN1002BOX). Electrophoresis was
780 performed at room temperature at 150 V for 90 min. Cathode buffer was swapped
781 from dark to light when the dye front was a third way through the gel. Separated
782 proteins were transferred to a nitrocellulose membrane by electrophoresis at 100 V for
783 90 min at 4 ℃.

784 Proteins were visualized using chemiluminescence. Secondary antibody (goat α-
785 rabbit, HRP;1:10,000; Abcam: ab6721). Chemiluminescence substrate SuperSignal
786 West Pico PLUS (ThermoScientific, ref number: 34579) according to manufacturer's
787 instructions. Chemiluminescence was detected using clear blue X-Ray Film CL-
788 Xposure™ Film (ThermoScientific, ref number: 34090).

789 **Chlorophyll fluorescence measurements in Chlamydomonas**

790 To measure PSII activity in Chlamydomonas, cells were grown in TAP in low light (20
791 µmol photons m^{-2} s^{-1}) for 4 days at 50 rpm to reach logarithmic phase. Cells were
792 then washed, resuspended to 30 µg Chl mL^{-1} in TP media and exposed to 150 µmol
793 photons m^{-2} s^{-1} light for 3 h, followed by 1 h incubation in darkness at 50 rpm before
794 recording Chl fluorescence using DUAL-PAM-100 (Walz, Effeltrich, Germany). A
795 saturating pulse of 3,000 µmol photons m^{-2} s^{-1} of 800 ms was applied to the samples
796 in a cuvette under continuous stirring for determination of the maximal fluorescence
797 yield in the dark state (F_m) and maximal fluorescence yield during the period with
798 actinic light (F_m'). The maximal photochemical efficiency of PSII (F_v/F_m) was
799 calculated. NPQ was determined from slow kinetics during actinic illumination at 1,500
800 µmol m^{-2} s^{-1} for 17 min followed by 5 min of dark relaxation. NPQ and Y(II) were
801 calculated based on changes in Chl fluorescence as $(F_m–F_m')/F_m'$ and $(F_m'–F)/ F_m'$,
802 respectively, according to Genty et al., (1989).

803 **Electrochromic shift (ECS) in Chlamydomonas**

804 ECS measurements in Chlamydomonas were carried out using a the Dual-PAM-100
805 equipped with a P515/535 module (Walz). Cells grown and prepared as for Chl
806 fluorescence experiments described previously were layered on a glass slide and
807 exposed to actinic red light for the given period. The light was switched off and decay
808 kinetics were measured. PMF size was calculated as the difference between the ECS
809 signal in light and the minimum value of the ECS signal immediately after the light was
810 turned off. Calculation of ΔpH and ΔΨ was performed using the steady-state time point

811 of the ECS signal in darkness (Cruz et al., 2001). Before each ECS measurement, a
812 3 saturating 50-µs actinic red flashes of 200,000 µmol photons m^{-2} s^{-1} was applied to
813 determine the ECS_{ST}; subsequently, the ECS_{ST} amplitude was used to normalize the
814 ECS signal before the calculation of PMF size and partitioning values. To determine
815 H^+ conductivity of the ATP synthase (g_{H^+}), the light was switched off at specific time
816 points to record the ECS signal decay during 620 ms dark intervals. The g_{H^+} parameter
817 was calculated as 1/τ (time constant for decay during the first 100 ms (Cruz et al.,
818 2005). The total proton flux across the membrane was calculated as v_{H^+} = PMF × g_{H^+}
819 (Cruz et al, 2001).

820 **Chlorophyll fluorescence measurements for Arabidopsis**

821 Plants were grown for 8 weeks on S-Hasselfors soil in a Percival AR-82L chamber
822 (CLF Plant Climatics, Wertingen, Germany) using 12 h light (180 µmol photons m^{-2}
823 s^{-1})/ 12h dark cycles at 21°C /19°C, respectively, and 70% relative humidity. Slow
824 kinetics of Chl *a* fluorescence induction were recorded with a pulse-amplitude
825 modulated fluorometer DUAL-PAM 100 equipped with DUAL-DB and DUAL-E emitter-
826 detector module (Walz) on attached leaves of 30 min dark-adapted plants using actinic
827 red light of 830 µmol photons m^{-2} s^{-1} for 10 min, followed by a 5 min dark period. The
828 saturating pulse applied was 5,000 µmol photons m^{-2} s^{-1} and of 800 ms duration. NPQ
829 and (Y(II)) were calculated based on changes in Chl fluorescence as $(F_m–F_m')/F_m'$ and
830 $(F_m'–F)/ F_m'$, respectively (Genty et al., 1989).

831 **Electrochromic shift (ECS) for Arabidopsis**

832 ECS was recorded with a DUAL-PAM 100 system equipped with a P515/535
833 emitter/detector module (Walz). First, plants were dark adapted for 30 min, then
834 illuminated with actinic red light at 830 µmol photons m^{-2} s^{-1} for 3 min followed by a
835 60 s dark period in which the ECS decay kinetics were recorded. Before each
836 measurement, three pulses of 5 µs and 200,000 µmol photons m^{-2} s^{-1} were applied to
837 determine ECS_{ST}, which was used to normalize the ECS_T values of each
838 measurement.

839 **Sedimentation of proto-pyrenoid**

840 Cross-linked samples were prepared by vacuum infiltrating intact leaves 1%
841 formaldehyde prior to sedimentation 200 mg of leaf tissue was flash frozen in liquid
842 nitrogen and ground by bead beating twice at 30 Hz for 30 s. Four times volume of

843 extraction buffer (50 mM HEPES-KOH pH 7.5, 17.4% (v/v) glycerol, 2% (v/v) Triton X-
844 100, cOmplete protease inhibitor tab) was added and sample mixed by bead beating
845 again. Extract was filtered through one layer of miracloth. A small aliquot of filtered
846 extract was saved as the input. Extract was then centrifuged at 500 x g for 3 min at 4
847 ℃ and the pellet discarded. The supernatant was centrifuged at 500 x g for 12min, 4
848 ℃. The pellet was washed once with extraction buffer and then centrifuged again. The
849 pellet was resuspended in 100 µl extraction buffer then centrifuged for a further 5 min.
850 Pellet was finally resuspended in 25 µl extraction buffer. Fractions were made up in
851 1x LDS loading buffer and 200 mM DTT. Ten microlitres was subjected to SDS-PAGE
852 (NuPAGE™ 4-12% Bis-Tris Mini Gel, Thermo Fisher, Catalogue number:
853 NP0322BOX) at 150 V for 60 min.

854 **Chloroplast fractionation**

855 In order to biochemically localize transgenically expressed BST4, chloroplasts were
856 fractionated as described in Herdean et al. (2016) using 100 g of leaf tissue from four-
857 five week-old BST4 transgenic plants. The stromal fraction was concentrated using a
858 10,000 MWCO centrifugal concentrator (Sartorius Stedim Biotech GmbH, product
859 number: VS1502).

860 **Electron microscopy of Chlamydomonas**

861 High (3%) and low (0.04%) CO_2 acclimated cells were harvested by centrifugation
862 (×1000g, 4 minutes, 20°C). Primary fixation was performed in 1.25% glutaraldehyde
863 in 50 mM sodium cacodylate (pH 7.15) in TP medium for 15 minutes followed by 2.5%
864 Glutaraldehyde in 50 mM cacodylate for 2 hours. Fixed samples were washed three
865 times with 50 mM sodium cacodylate by centrifugation. Samples were then osmicated
866 with 1% OsO4 in 50 mM sodium 25 cacodylate for 1 hour on ice and washed with de-
867 ionised water. Samples were block stained in 1% uranyl acetate in the dark for 1 hour.
868 Samples were washed twice with dH_2O and twice with 50 mM sodium cacodylate.
869 Fixed samples were dehydrated in an acetone series (25%, 50%, 75%, 90% and
870 100%) ~20 minutes each step. Dehydrated samples were infiltrated with Spurr's resin
871 by incubating in 25% then 50% Spurr resin in acetone for 30 minutes and transferred
872 to 75% for 45 minutes at room temperature. They were then incubated in 100% Spurr
873 resin overnight before polymerising at 70 °C for 24 hours. Sections ~70 nm thick were

874 collected on Copper grids and stained with saturated uranyl acetate and lead citrate.
875 Images were collected with a FEI Tecnai 12 BT at 120kV using a Ceta camera.

876 **Electron microscopy of Arabidopsis**

877 Leaves were cut into small 5 mm strips and fixed in 4% (v/v) Paraformaldehyde/0.5%
878 glutaraldehyde in 0.05M sodium cacodylate (pH = 7.2) by vacuum infiltration three
879 times for 15 min and incubation at 4 °C overnight with gentle agitation followed by
880 dehydration in increasing amounts of ethanol 50/70/80/90/100% 1 hr each then
881 overnight rotation. 100% ethanol was repeated 3 times, 1 hr each and a final over
882 night at 4 °C. Samples were then fixed in LR resin by infiltrating with increasing
883 concentration (50/70/100%) with a repeat of 100% and then polymerised overnight at
884 50 °C. Ultrathin sections were cut and mounted onto plastic-coated copper grids. Grids
885 were stained with 2% uranyl acetate and visualized by transmission electron
886 microscopy (TEM).

887 **Protease protection assay**

888 Investigation of the orientation of BST4 in isolated thylakoid membranes was
889 conducted as described in Stepien and Johnson (2018). Briefly, trypsin made up in 50
890 mM acetic acid according to the manufacturer's instructions (Thermo Scientific, ref
891 number: 90057). To disrupt the thylakoid membrane and allow degradation to lumen-
892 facing peptides, 1% (v/v) Triton X-100 was added, and tubes gently agitated prior to
893 addition of trypsin.

894 **Xenopus oocyte electrophysiology**

895 Destination clones containing BST4 for Xenopus expression were linearized with
896 EcoRI, before proceeding to the *in vitro* transcription (mMessage mMachine T7
897 transcription kit, Thermofisher Scientific, ref number AM1344). Stage IV oocytes were
898 injected with 20 ng of RNA per oocyte. Measurements of ion transport was done by
899 voltage clamp using an Axoclamp 2B amplifier (Axon instruments, Foster City, CA)
900 (Lefoulon et al., 2014; Leyman et al., 1999). They were performed under perfusion of
901 either 100 mM KCl, K-HCO_3, Na-HCO_3, K-PEP, or K-Gluconate, with 1 mM $CaCl_2$, 1.5
902 mM $MgCl_2$, and 10 mM HEPES-NaOH, pH 7.3. Recordings were obtained and
903 analysed using Henry IV software (Y-Science, Glasgow, UK). BST4 expression in
904 oocytes was validated by western blotting (Fig S10B), as described above.

ACKNOWLEDGEMENTS

The authors thank the University of York Horticulture team who helped with setting up the Chlamydomonas phototaxis assays. TEM for Arabidopsis was carried out with the support of Stephen Mitchell and the Wellcome Trust Multi User Equipment Grant (WT104915MA)

For the purpose of open access, a Creative Commons Attribution (CC BY) licence is applied to any Author Accepted Manuscript version arising from this submission.

AUTHOR CONTRIBUTIONS

LA, CW, CSL, CS, AM and LM conceived and designed the study with input from all authors. LA performed all Arabidopsis experiments, BN-PAGE and immunoblots. CW performed Chlamydomonas physiology experiments and immunoblots. CSL performed Chlamydomonas microscopy imaging and immunoblots. KMS, KAvM, and ED performed Chlamydomonas and Arabidopsis Chl fluorescence and ECS experiments and generated figures. APD and CW performed molecular tracking experiments with input from ML. CL and MB performed xenopus oocyte work. PG and JB did *in silico* structure predictions. TEM contributed to the complementation of Chlamydomonas *bst4* mutant. NA contributed to Arabidopsis transgenic line generation. GP assisted with experimental design and data interpretation. LA and CW generated figures. LA led the writing of the manuscript with input from CW. All other authors provided manuscript feedback.

REFERENCES

Adler L, Díaz-Ramos A, Mao Y, Pukacz KR, Fei C, Mccormick AJ (2022) New horizons for building pyrenoid-based CO_2 -concentrating mechanisms in plants to improve yields. Plant Physiol 190: 1609-1627

Aro E-M, Rokka A, Vener A V (2004) Determination of Phosphoproteins in Higher Plant Thylakoids BT - Photosynthesis Research Protocols. *In* R Carpentier, ed,Humana Press, Totowa, NJ, pp 271–285

Atkinson N, Feike D, Mackinder LCM, Meyer MT, Griffiths H, Jonikas MC, Smith AM, Mccormick AJ (2016) Introducing an algal carbon-concentrating mechanism into higher plants: Location and incorporation of key components. Plant Biotechnol J 14: 1302–1315

Atkinson N, Leitão N, Orr DJ, Meyer MT, Carmo-Silva E, Griffiths H, Smith AM, McCormick AJ (2017) Rubisco small subunits from the unicellular green alga Chlamydomonas complement Rubisco-deficient mutants of Arabidopsis. New

942 Phytol 214: 655–667
943 Atkinson N, Mao Y, Chan KX, McCormick AJ (2020) Condensation of Rubisco into a
944 proto-pyrenoid in higher plant chloroplasts. Nat Commun 11: 6303
945 Bergner SV, Scholz M, Trompelt K, Barth J, Gäbelein P, Steinbeck J, Xue H, Clowez
946 S, Fucile G, Fufezan C, et al (2015) STATE TRANSITION7-Dependent
947 Phosphorylation Is Modulated by Changing Environmental Conditions , and Its
948 Absence Triggers Remodeling of Photosynthetic Protein Complexes 1. Plant
949 Physiol *168*: 615-634
950 Bharill S, Fu Z, Palty R, Isacoff EY (2014) Stoichiometry and specific assembly of
951 Best ion channels. Proc Natl Acad Sci U S A 111: 6491–6496
952 Burlacot A, Dao O, Auroy P, Cuiné S, Li-Beisson Y, Peltier G (2022) Alternative
953 photosynthesis pathways drive the algal CO_2-concentrating mechanism. Nature
954 605: 366–371
955 Caspari OD, Meyer MT, Tolleter D, Wittkopp TM, Cunniffe NJ, Lawson T, Grossman
956 AR, Griffiths H (2017) Pyrenoid loss in *Chlamydomonas reinhardtii* causes
957 limitations in CO_2 supply, but not thylakoid operating efficiency. J Exp Bot 68:
958 3903–3913
959 Choi BY, Kim H, Shim D, Jang S, Yamaoka Y, Shin S, Yamano T, Kajikawa M, Jin
960 ES, Fukuzawa H, et al (2022) The Chlamydomonas bZIP transcription factor
961 BLZ8 confers oxidative stress tolerance by inducing the carbon-concentrating
962 mechanism. Plant Cell 34: 910–926
963 Ciorba MA, Heinemann SH, Weissbach H, Brot N, Hoshi T (1999) Regulation of
964 voltage-dependent K^+ channels by methionine oxidation: effect of nitric oxide
965 and vitamin C. FEBS Lett 442: 48–52
966 Cruz JA, Avenson TJ, Kanazawa A, Takizawa K, Edwards GE, Kramer DM (2005)
967 Plasticity in light reactions of photosynthesis for energy production and
968 photoprotection. J Exp Bot 56: 395–406
969 Cruz JA, Sacksteder CA, Kanazawa A, Kramer DM (2001) Contribution of electric
970 field (Δψ) to steady-state transthylakoid proton motive force (pmf) in vitro and in
971 vivo. Control of pmf parsing into Δψ and ΔpH by ionic strength. Biochemistry 40:
972 1226–1237
973 Emrich-Mills TZ, Yates G, Barrett J, Girr P, Grouneva I, Lau CS, Walker CE, Kwok
974 TK, Davey JW, Johnson MP, et al (2021) A recombineering pipeline to clone
975 large and complex genes in Chlamydomonas. Plant Cell 33: 1161–1181
976 Engel BD, Schaffer M, Kuhn Cuellar L, Villa E, Plitzko JM, Baumeister W (2015)
977 Native architecture of the Chlamydomonas chloroplast revealed by in situ cryo-
978 electron tomography. Elife 4: e11383
979 Engler C, Youles M, Gruetzner R, Ehnert T-M, Werner S, Jones JDG, Patron NJ,
980 Marillonnet S (2014) A Golden Gate Modular Cloning Toolbox for Plants. ACS
981 Synth Biol 3: 839–843
982 Erickson E, Wakao S, Niyogi KK (2015) Light stress and photoprotection in
983 *Chlamydomonas reinhardtii*. Plant J 82: 449–465
984 Fei C, Wilson AT, Mangan NM, Wingreen NS, Jonikas MC (2022) Modelling the
985 pyrenoid-based CO_2-concentrating mechanism provides insights into its
986 operating principles and a roadmap for its engineering into crops. Nat Plants 8:
987 583–595
988 Genkov T, Meyer M, Griffiths H, Spreitzer RJ (2010) Functional hybrid rubisco
989 enzymes with plant small subunits and algal large subunits: Engineered rbcS
990 cDNA for expression in chlamydomonas. J Biol Chem 285: 19833–19841
991 Genty B, Briantais JM, Baker NR (1989) The relationship between the quantum yield

992 of photosynthetic electron transport and quenching of chlorophyll fluorescence.
993 Biochim Biophys Acta - Gen Subj 990: 87–92
994 Grefen C, Chen Z, Honsbein A, Donald N, Hills A, Blatt MR (2010) A Novel Motif
995 Essential for SNARE Interaction with the K^+ Channel KC1 and Channel Gating
996 in Arabidopsis . Plant Cell 22: 3076–3092
997 Guindon S, Dufayard J-F, Lefort V, Anisimova M, Hordijk W, Gascuel O (2010) New
998 Algorithms and Methods to Estimate Maximum-Likelihood Phylogenies:
999 Assessing the Performance of PhyML 3.0. Syst Biol 59: 307–321
1000 Hagino T, Kato T, Kasuya G, Kobayashi K, Kusakizako T, Hamamoto S, Sobajima T,
1001 Fujiwara Y, Yamashita K, Kawasaki H, et al (2022) Cryo-EM structures of
1002 thylakoid-located voltage-dependent chloride channel VCCN1. Nat Commun 13:
1003 2505
1004 Hasegawa M, Shiina T, Terazima M, Kumazaki S (2010) Selective excitation of
1005 photosystems in chloroplasts inside plant leaves observed by near-infrared
1006 laser-based fluorescence spectral microscopy. Plant Cell Physiol 51: 225–238
1007 He S, Chou H, Matthies D, Wunder T, Meyer MT, Martinez-sanchez A, Jeffrey PD,
1008 Port SA, He G, Chen VK, et al (2020) The Structural Basis of Rubisco Phase
1009 Separation in the Pyrenoid. 6: 1480–1490
1010 Hennacy JH, Jonikas MC (2020) Prospects for Engineering Biophysical CO_2
1011 Concentrating Mechanisms into Land Plants to Enhance Yields. Annu Rev Plant
1012 Biol 71: 461-485
1013 Herdean A, Teardo E, Nilsson AK, Pfeil BE, Johansson ON, Ünnep R, Nagy G,
1014 Zsiros O, Dana S, Solymosi K, et al (2016) A voltage-dependent chloride
1015 channel fine-tunes photosynthesis in plants. Nat Commun 7: 11654
1016 Horton P, Long SP, Smith P, Banwart SA, Beerling DJ (2021) Technologies to
1017 deliver food and climate security through agriculture. Nat Plants 7: 250–255
1018 Hunter P, Payne-Dwyer AL, Shaw M, Signoret N, Leake MC (2022) Single-molecule
1019 and super-resolved imaging deciphers membrane behavior of onco-
1020 immunogenic CCR5. iScience 25: 105675
1021 Izumi M, Tsunoda H, Suzuki Y, Makino A, Ishida H (2012) RBCS1A and RBCS3B,
1022 two major members within the Arabidopsis RBCS multigene family, function to
1023 yield sufficient Rubisco content for leaf photosynthetic capacity. J Exp Bot 63:
1024 2159–2170
1025 Karlsson J, Ciarke AK, Chen ZY, Hugghins SY, Park Y II, Husic HD, Moroney J V.,
1026 Samuelsson G (1998) A novel α-type carbonic anhydrase associated with the
1027 thylakoid membrane in *Chlamydomonas reinhardtii* is required for growth at
1028 ambient CO_2. EMBO J 17: 1208–1216
1029 Katoh K, Standley DM (2013) MAFFT Multiple Sequence Alignment Software
1030 Version 7: Improvements in Performance and Usability. Mol Biol Evol 30: 772–
1031 780
1032 Le SQ, Gascuel O (2008) An Improved General Amino Acid Replacement Matrix.
1033 Mol Biol Evol 25: 1307–1320
1034 Lee S, Yoon B-E, Berglund K, Oh S-J, Park H, Shin H-S, Augustine GJ, Lee CJ
1035 (2010) Channel-mediated tonic GABA release from glia. Science 330: 790–796
1036 Lefoulon C, Waghmare S, Karnik R, Blatt MR (2018) Gating control and K^+ uptake by
1037 the KAT1 K^+ channel leaveraged through membrane anchoring of the trafficking
1038 protein SYP121. Plant Cell Environ 41: 2668–2677
1039 Li X, Zhang R, Patena W, Gang SS, Blum SR, Ivanova N, Yue R, Robertson JM,
1040 Lefebvre PA, Fitz-Gibbon ST, et al (2015) An indexed, mapped mutant library
1041 enables reverse genetics studies of biological processes in chlamydomonas

reinhardtii. Plant Cell 28: 367–387
Long S, Burgess S, Causton I (2019) Redesigning Crop Photosynthesis. Sustain. Glob. Food Secur. Nexus Sci. Policy. pp 131–141
Ma Y, Pollock S V., Xiao Y, Cunnusamy K, Moroney J V. (2011) Identification of a novel gene, *CIA6*, required for normal pyrenoid formation in *Chlamydomonas reinhardtii*. Plant Physiol 156: 884–896
Mackinder LCM, Chen C, Leib RD, Patena W, Blum SR, Rodman M, Ramundo S, Adams CM, Jonikas MC (2017) A Spatial Interactome Reveals the Protein Organization of the Algal CO_2-Concentrating Mechanism. Cell 171: 133–147
McGrath JM, Long SP (2014) Can the cyanobacterial carbon-concentrating mechanism increase photosynthesis in crop species? A theoretical analysis. Plant Physiol 164: 2247–2261
Meyer MT, Itakura AK, Patena W, Wang L, He S, Emrich-Mills T, Lau CS, Yates G, MacKinder LCM, Jonikas MC (2020) Assembly of the algal CO_2-fixing organelle, the pyrenoid, is guided by a Rubisco-binding motif. Sci Adv 6: eabd2408
Minh BQ, Schmidt HA, Chernomor O, Schrempf D, Woodhams MD, von Haeseler A, Lanfear R (2020) IQ-TREE 2: New Models and Efficient Methods for Phylogenetic Inference in the Genomic Era. Mol Biol Evol 37: 1530–1534
Mukherjee A, Lau CS, Walker CE, Rai AK, Prejean CI, Yates G, Emrich-Mills T, Lemoine SG, Vinyard DJ, Mackinder LCM, et al (2019) Thylakoid localized bestrophin-like proteins are essential for the CO_2 concentrating mechanism of Chlamydomonas reinhardtii. Proc Natl Acad Sci U S A 116: 16915–16920
Payne-Dwyer AL, Leake MC (2022) Single-Molecular Quantification of Flowering Control Proteins Within Nuclear Condensates in Live Whole Arabidopsis Root BT - Chromosome Architecture: Methods and Protocols. *In* MC Leake, ed,Springer US, New York, NY, pp 311–328
Payne-Dwyer AL, Syeda AH, Shepherd JW, Frame L, Leake MC (2022) RecA and RecB: probing complexes of DNA repair proteins with mitomycin C in live Escherichia coli with single-molecule sensitivity. J R Soc Interface 19: 20220437
Plank M, Wadhams GH, Leake MC (2009) Millisecond timescale slimfield imaging and automated quantification of single fluorescent protein molecules for use in probing complex biological processes. Integr Biol (Camb) 1: 602–612
Price GD, Pengelly JJL, Forster B, Du J, Whitney SM, von Caemmerer S, Badger MR, Howitt SM, Evans JR (2013) The cyanobacterial CCM as a source of genes for improving methylation and chromatin patterning photosynthetic CO_2 fixation in crop species. J Exp Bot 64: 753–768
Qu Z, Cui Y, Hartzell C (2006) A short motif in the C-terminus of mouse bestrophin 4 inhibits its activation as a Cl^- channel. FEBS Lett 580: 2141–2146
Qu Z, Hartzell HC (2008) Bestrophin Cl^- channels are highly permeable to HCO_3^- . Am J Physiol Physiol 294: C1371–C1377
Roberts SK, Milnes J, Caddick M (2011) Characterisation of *An*BEST1 , a functional anion channel in the plasma membrane of the filamentous fungus , *Aspergillus nidulans*. Fungal Genet Biol 48: 928–938
Santhanagopalan I, Wong R, Mathur T, Griffiths H (2021) Orchestral manoeuvres in the light: Crosstalk needed for regulation of the Chlamydomonas carbon concentration mechanism. J Exp Bot 72: 4604–4624
Schindelin J, Arganda-Carreras I, Frise E, Kaynig V, Longair M, Pietzsch T, Preibisch S, Rueden C, Saalfeld S, Schmid B, et al (2012) Fiji: an open-source platform for biological-image analysis. Nat Methods 9: 676–682
Shepherd JW, Payne-Dwyer AL, Lee JE, Syeda A, Leake MC (2021) Combining

1092 single-molecule super-resolved localization microscopy with fluorescence
1093 polarization imaging to study cellular processes. JPhys Photonics. 3: 034010
1094 Stepien P, Johnson GN (2018) Plastid terminal oxidase requires translocation to the
1095 grana stacks to act as a sink for electron transport. Proc Natl Acad Sci U S A
1096 115: 9634–9639
1097 Sueoka N (1960) Mitotic Replication of Deoxyribonucleic Acid in Chlamydomonas
1098 Reinhardi. Proc Natl Acad Sci 46: 83–91
1099 Syeda AH, Wollman AJM, Hargreaves AL, Howard JAL, Brüning J-G, McGlynn P,
1100 Leake MC (2019) Single-molecule live cell imaging of Rep reveals the dynamic
1101 interplay between an accessory replicative helicase and the replisome. Nucleic
1102 Acids Res 47: 6287–6298
1103 Tardif M, Atteia A, Specht M, Cogne G, Rolland N, Brugière S, Hippler M, Ferro M,
1104 Bruley C, Peltier G, et al (2012) PredAlgo: a new subcellular localization
1105 prediction tool dedicated to green algae. Mol Biol Evol 29: 3625–3639
1106 Ueki N, Ide T, Mochiji S, Kobayashi Y, Tokutsu R, Ohnishi N, Yamaguchi K,
1107 Shigenobu S, Tanaka K, Minagawa J, et al (2016) Eyespot-dependent
1108 determination of the phototactic sign in *Chlamydomonas reinhardtii*. Proc Natl
1109 Acad Sci U S A 113: 5299–5304
1110 Wollman AJM, Fournier C, Llorente-Garcia I, Harriman O, Payne-Dwyer AL,
1111 Shashkova S, Zhou P, Liu T-C, Ouaret D, Wilding J, et al (2022) Critical roles for
1112 EGFR and EGFR–HER2 clusters in EGF binding of SW620 human carcinoma
1113 cells. J R Soc Interface 19: 20220088
1114 Woo DH, Han K-S, Shim JW, Yoon B-E, Kim E, Bae JY, Oh S-J, Hwang EM,
1115 Marmorstein AD, Bae YC, et al (2012) TREK-1 and Best1 Channels Mediate
1116 Fast and Slow Glutamate Release in Astrocytes upon GPCR Activation. Cell
1117 151: 25–40
1118 Wu A, Brider J, Busch FA, Chen M, Chenu K, Clarke VC, Collins B, Ermakova M,
1119 Evans JR, Farquhar GD, et al (2023) A cross-scale analysis to understand and
1120 quantify the effects of photosynthetic enhancement on crop growth and yield
1121 across environments. Plant Cell Environ 46: 23–44
1122 Yang T, Liu Q, Kloss B, Bruni R, Kalathur RC, Guo Y, Kloppmann E, Rost B,
1123 Colecraft HM, Hendrickson WA (2014) Structure and selectivity in bestrophin ion
1124 channels. Science 346: 355–359
1125 Zhang R, Patena W, Armbruster U, Gang SS, Blum SR, Jonikas MC (2014) High-
1126 throughput genotyping of green algal mutants reveals random distribution of
1127 mutagenic insertion sites and endonucleolytic cleavage of transforming DNA.
1128 Plant Cell 26: 1398–1409

Supplemental Figures

0.04% CO_2							
		Days 0-3			**Days 0 to 5**		
	Strain	Mean	SE	*P(T<=t)* two-tail	Mean	SE	*P(T<=t)* two-tail
SGR (μ h^{-1})	WT	0.0389	0.0007		0.0241	0.0010	
	bst4	0.0402	0.0003	0.1652	0.0257	0.0001	0.2036
Doubling time (h)	WT	17.8462	0.3380		28.8436	1.2467	
	bst4	17.2379	0.1255	0.1669	26.9798	0.1491	0.2119
3% CO_2							
		Days 0-2			**Days 0-3**		
	Strain	Mean	SE	*P(T<=t)* two-tail	Mean	SE	*P(T<=t)* two-tail
SGR (μ h^{-1})	WT	0.0679	0.0013		0.0456	0.0011	
	bst4	0.0682	0.0010	0.8626	0.0455	0.0003	0.9436
Doubling time (h)	WT	10.2145	0.1930		15.2239	0.3725	
	bst4	10.1669	0.1510	0.8555	15.2353	0.0878	0.9777

Supplemental Table 1 compares specific growth rates (μ h^{-1}) and cell doubling times of WT and *bst4* strains (n=3) during liquid growth assays at 0.04 and 3 % CO_2.

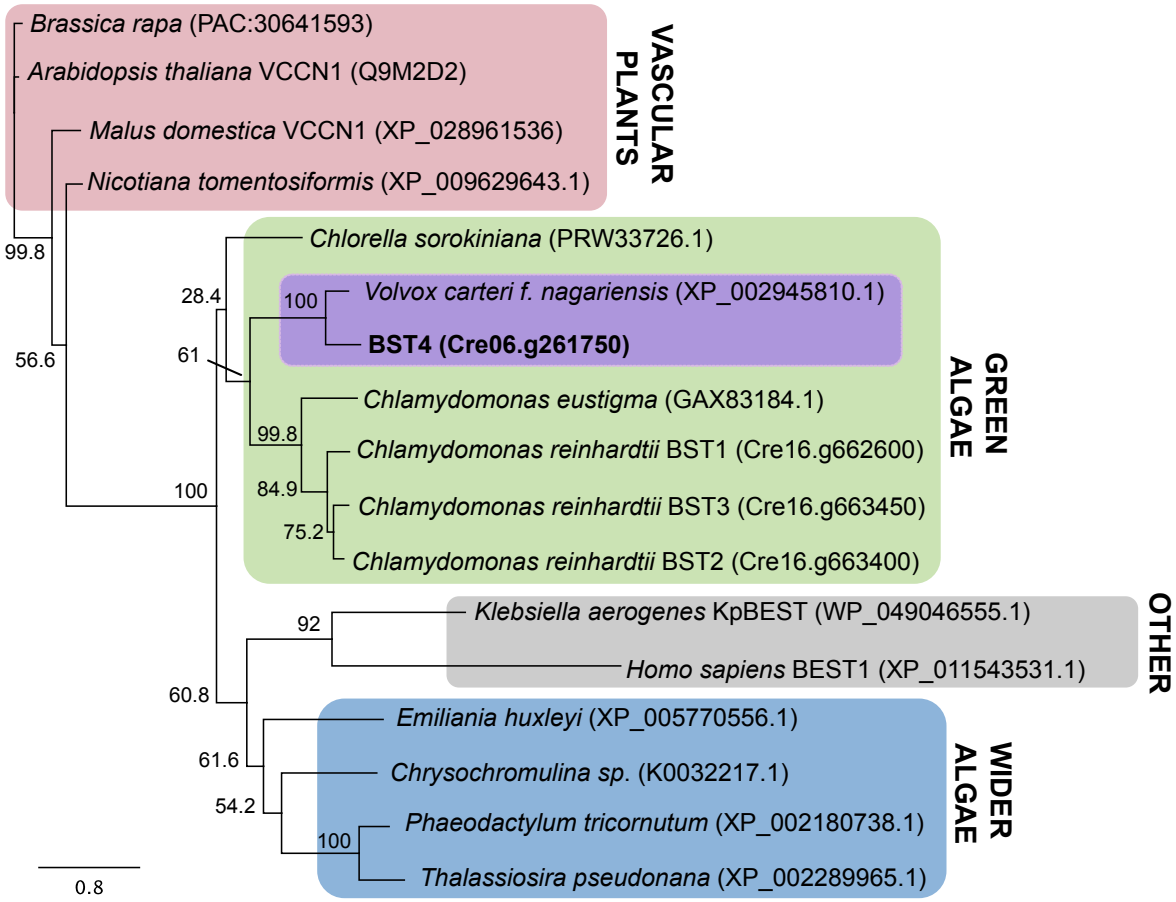

Supplemental Figure 1. BST4 structure and sequence compared to other bestrophins. Phylogenetic analysis of the full length Chlamydomonas BST4 amino acid sequence (bold). The evolutionary history of BST4 was inferred by using the maximum likelihood method based on the Le and Gascuel substitution model with discrete Gamma distribution (5 categories) and 500 bootstrap replicates. The tree is drawn to scale, with branch lengths measured in the number of substitutions per site.

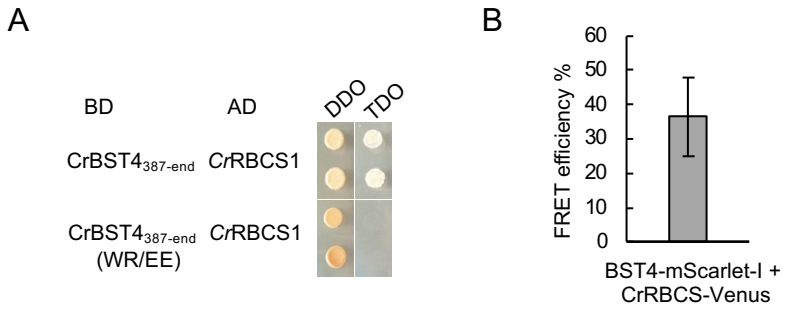

Supplemental Figure 2. Interaction between BST4 and RBCS. A. Yeast-2-hybrid experiment. The disordered region of BST4 C-terminus (a.a 387-end) and with residues WR from RBMs are changed to EE. Abbreviations: AD, activation domain; BD, binding domain; DDO, double drop out media; TDO, triple drop out media **B**. FRET efficiency between BST4-mScarlet-I and CrRBCS-Venus. Sensitized-FRET measurement on dual-tagged cells (BST4-Venus and RBCS1-mCherry) showed a moderate FRET efficiency of 35% (n=10).

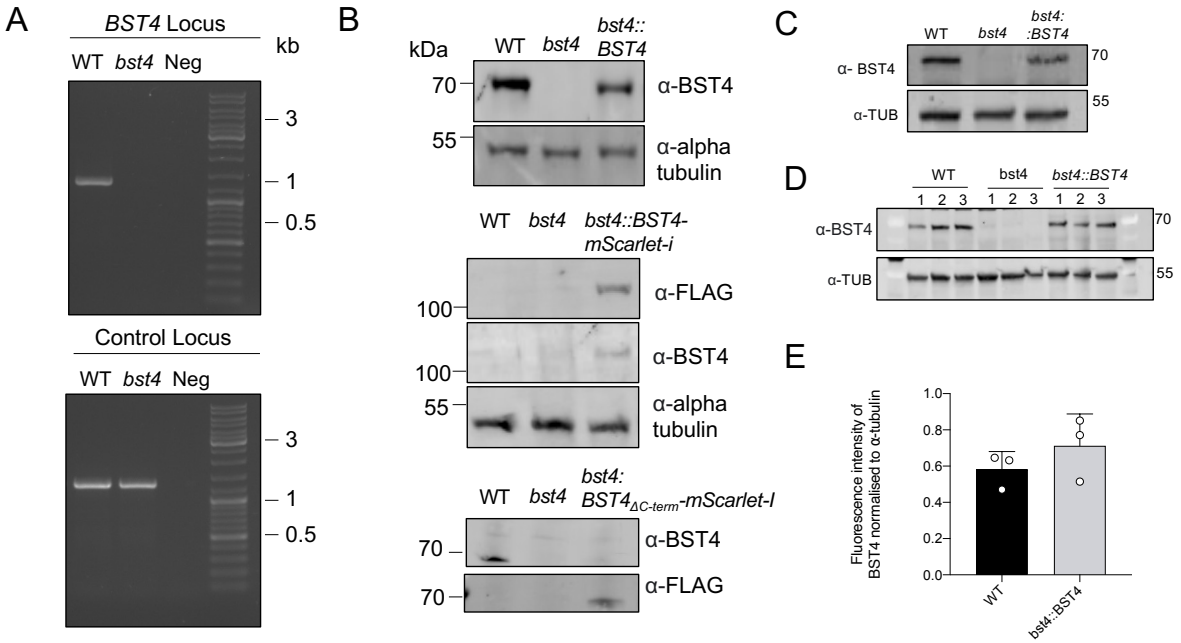

Supplemental Figure 3. Validation of Chlamydomonas BST4 lines. **A.** PCR amplification of the *BST4* and control loci of WT (CMJ030 (CC-4533; cw15, mt -) and *bst4* (LMJ.RY0402.159478) gDNA to confirm the insertion of the CIB1 cassette in *bst4.* **B.** Immunoblots confirming the production of BST4 in WT, *bst4, bst4::BST4* and *bst4::BST-truncated* Chlamydomonas lines. **C.** Immunoblot showing the absence of BST4 in the *bst4* knock-out line and presence in the WT and *bst4::BST4* complemented lines. **D.** Western blot used to quantify the amount of BST4 protein detected in WT and *bst4::BST4.* **E.** Immunoblot was used for the quantification of fluorescent intensity as a measure of BST4 protein abundance. All fluorescent intensity measurements were normalized to respective alpha-tubulin loading controls and conducted in triplicate. No statistical difference was observed between WT and *bst4::BST4* BST4 protein abundance (Paired two-tail t-test p = 0.22, n=3)

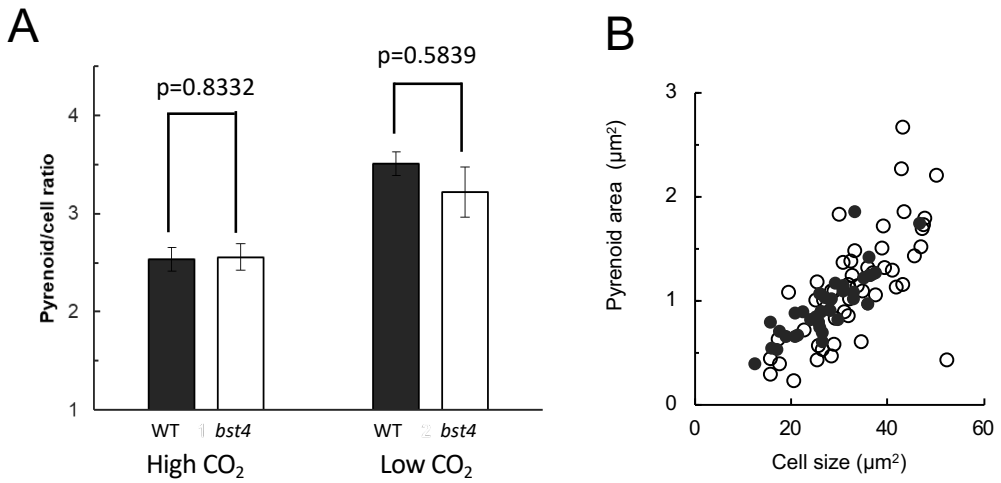

Supplemental Figure 4. Pyrenoid morphology in *bst4* vs WT. A. The pyrenoid area to cell area ratio of wild type (black) and *bst4* (white) strains at high (3%) and low (0.04%) CO_2 concentrations. Each bar represents the mean value ± SEM (n=40–50). The data for wild type and *bst4* strains were compared using a two sample T-test. The p-values (showing no significant difference) are displayed above the bars. **B.** Pyrenoid area vs cell size of WT and bst4 at 0.04% [CO_2].

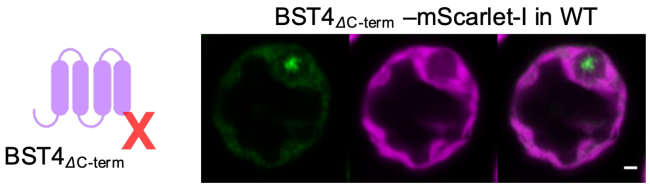

Supplemental Figure 5. Localisation of C-terminally truncated BST4 in WT background. BST4$_{\Delta Cterm}$-mScarlet-I fluorescence shown in green and chlorophyll autofluorescence in magenta. Scale is bar 1 µm.

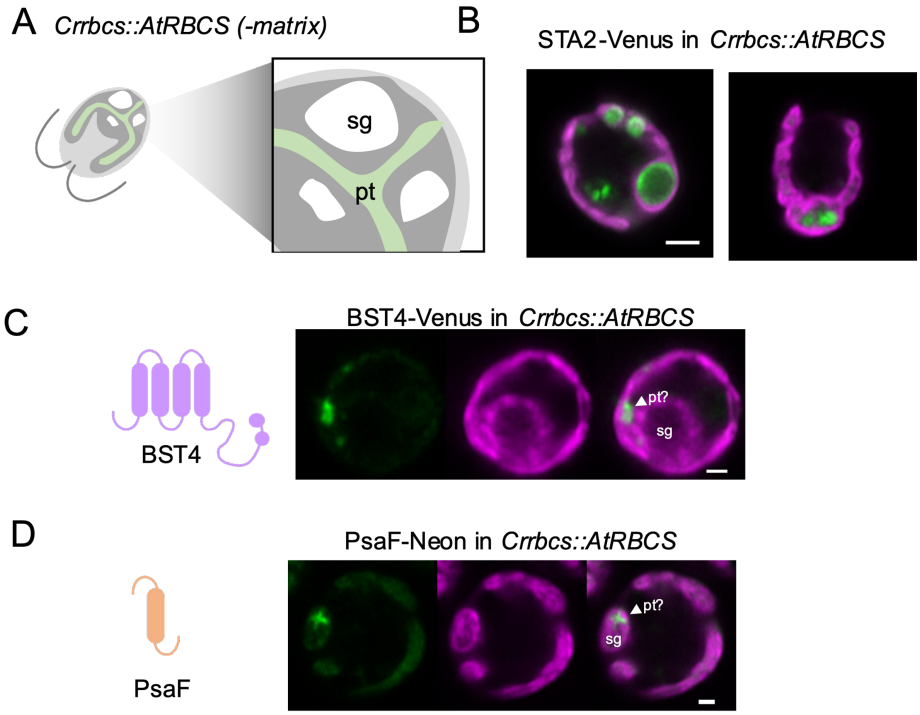

Supplemental Figure 6. Localisation of proteins in a pyrenoid matrix-less background. A. Diagram showing a section of the *Crrbcs::AtRBCS* matrix-less mutant (*-matrix*). The nascent pyrenoid tubules (pt) are shown in dark green, starch granules (sg) in white. **B.** Confocal image of starch binding protein STA2 fused to Venus in *Crrbcs::AtRBCS.* Scale bar is 2 µm. **C.** BST4-Venus in a WT Chlamydomonas cell. Scale bar is 1 µm. **D.** PsaF-mNeon in *Crrbcs::AtRBCS*. Venus and mNeonGreen fluorescence are shown in green and chlorophyll autofluorescence in magenta. Scale bar is 1 µm.

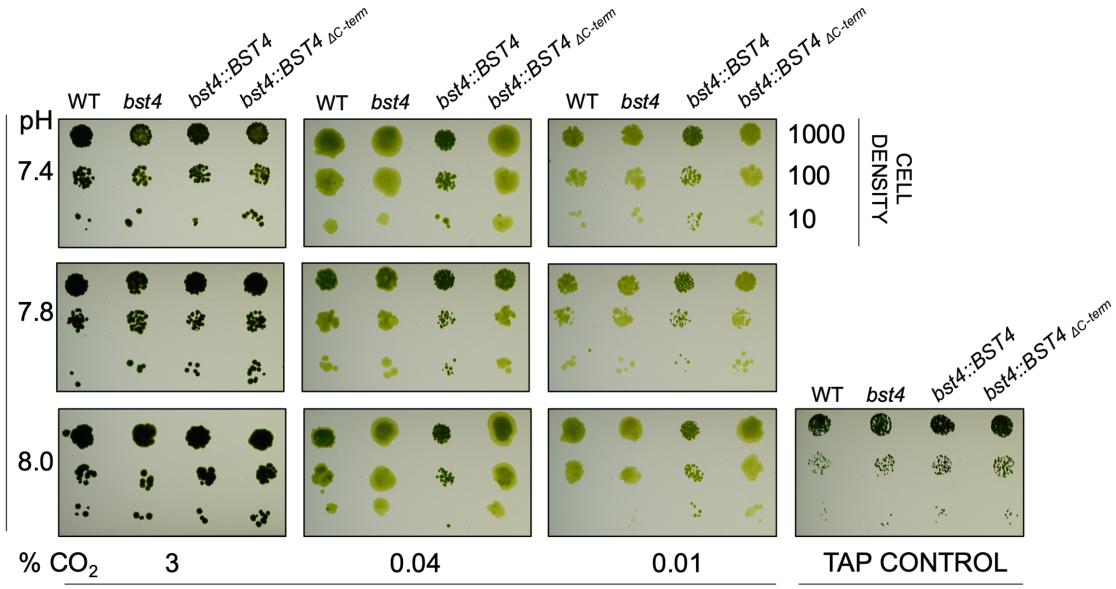

Supplemental Figure 7. Spot test of WT, *bst4* and BST4 complemented lines under CCM induced conditions. *Chlamydomonas* strains were grown in serial dilution on agar plates in saturating light (400 µmol m^{-2} s^{-1}) under a range of CO_2 and pH conditions (specified) to induce the CCM. All lines grew comparably to WT across the conditions used and on the low light TAP control plate.

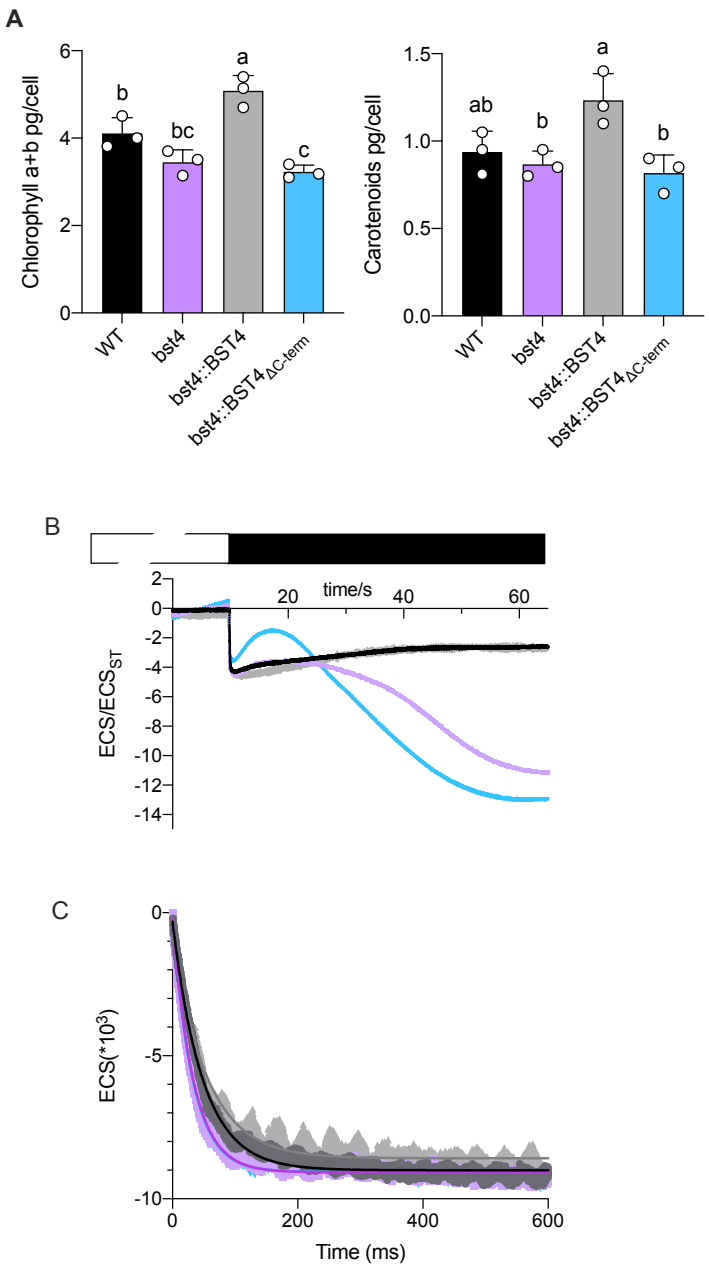

Supplemental Figure 8. **Photosynthetic parameters of WT Chlamydomonas and mutants.** Wild type (WT) and mutants were grown on TAP medium in the light at 20 µmol photons m^{-2} s^{-1}. **A.** Chlorophyll and carotenoid contents of cells were determined in methanol extracts. **B.** In a separate experiment, cells resuspended in TP at 30 µg Chl ml^{-1} were dark-adapted for 1 h and then illuminated for 10 min with 530 µmol photons m^{-2} s^{-1} after which the light was switched off to record ECS in darkness. **C.** Representative Electrochromic shift (ECS) decay curves. The cells were prepared as in B. To determine the g_{H^+} parameter, ECS kinetics were recorded during 600 ms dark intervals. The ECS decay of the first 100 ms was fitted to calculate g_{H^+} (s^{-1}) =1/time constant for decay. Data are the means ±SEM (n=3 replicates).

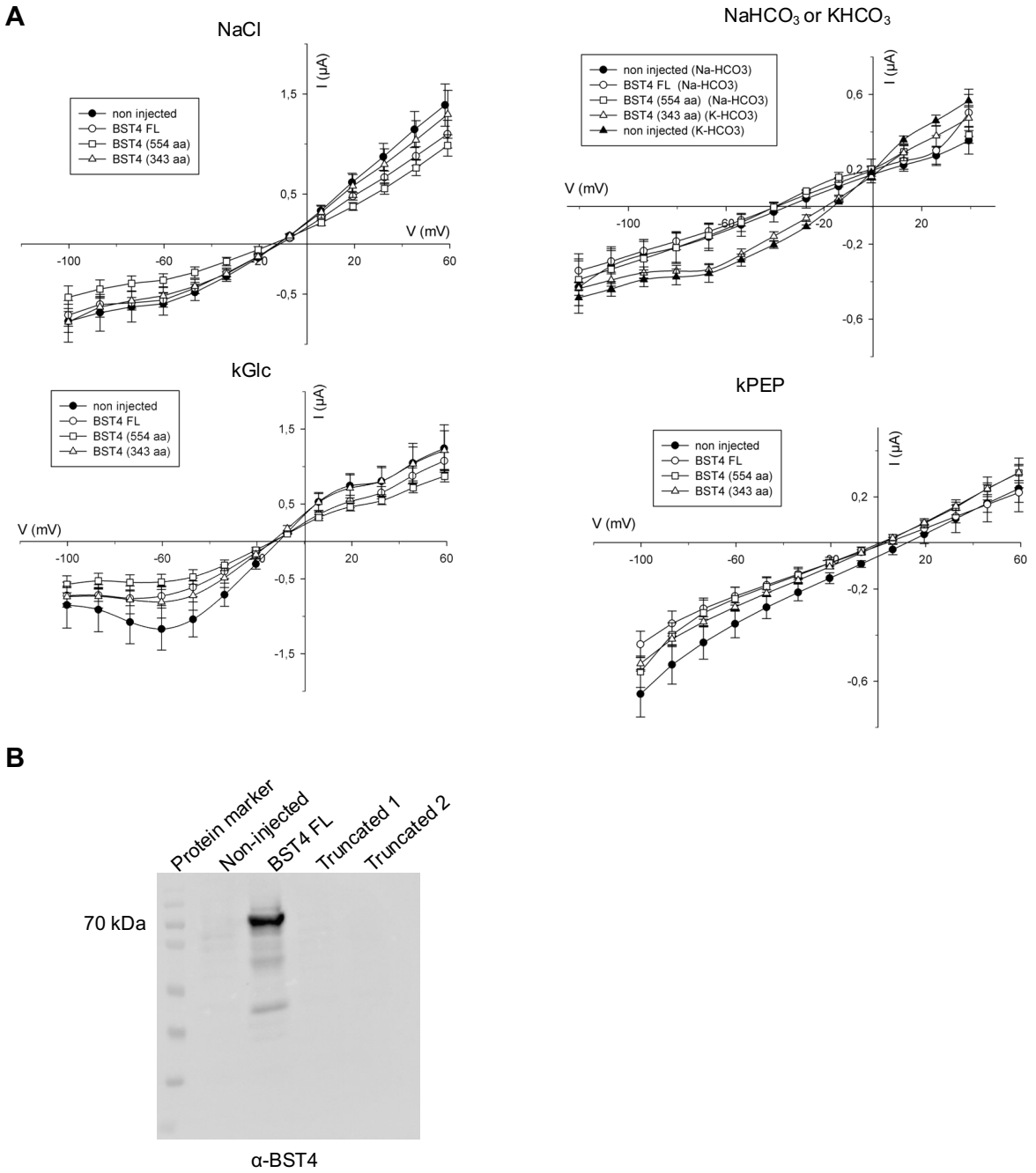

Supplemental Figure 9. No currents were detected for BST4 with any anions tested in Xenopus oocytes A. Steady state currents analysis of oocytes injected with BST4, full length or truncated, compared to non-injected oocytes. The voltage steps start from 60 mV to -100 mV (Cl^-, PEP^-, and Gluconate conditions) 40 mV to -120 mV ($HCO3^-$ conditions, right panel), holding voltage is -20 mV. Recordings were performed on n>4 oocytes. There is no differences between the currents recorded in non-injected oocytes and expressing the protein. **B.** Western Blot analysis of oocytes. Lane 1 is the marker, lane 2 are non-injected oocytes, lane 3 is the full-length protein (about 66 kDa), lanes 3 and 4 are the truncated proteins. We can only detect full length BST4 as the antibody is directed against the C-terminal part of the protein that is removed in the two truncated versions of the channel.

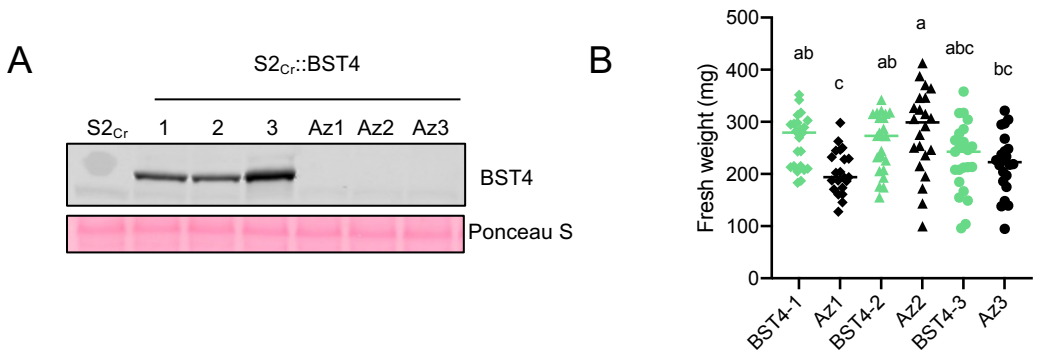

Supplemental Figure 10. Phenotype of BST4 transgenic Arabidopsis line. A. Immunoblot against BST4 of proteins extracted from BST4 no tag lines and Azygous segregants (Az). $S2_{Cr}$ is the parent line. **B.** Fresh weight of 28-day old rosettes, bars represent mean weight for each genotype n=18-21. Different letters indicate statistically significant difference among the genotypes (one-way ANOVA test, followed by Turkey's post hoc test, $P < 0.05$).

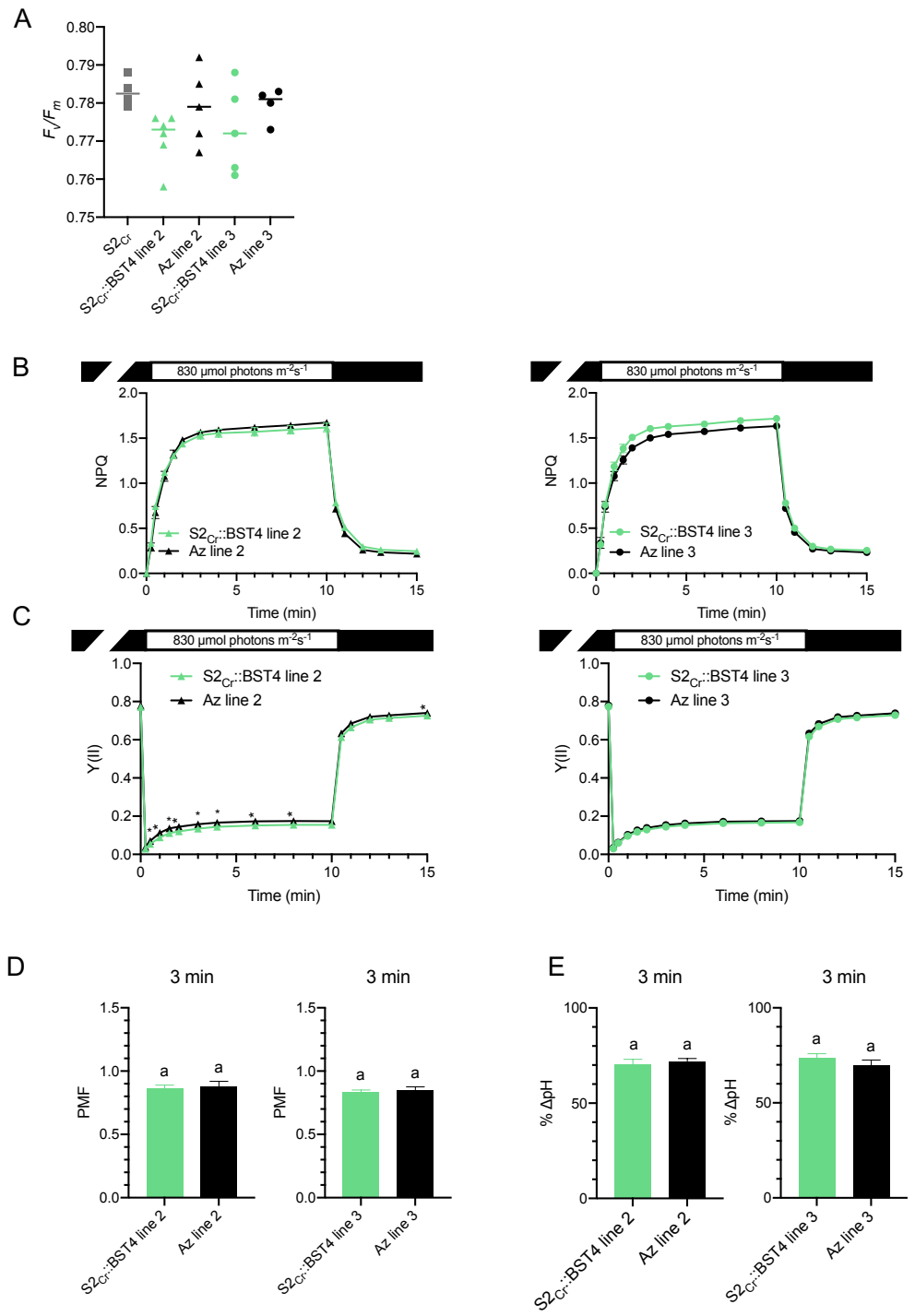

Supplemental Figure 11. Photosynthetic measurements of BST4 transgenic Arabidopsis lines 2 and 3. A. F_v/F_m values measured on attached, 30 min dark adapted leaves of 8-week-old plants (n=15-21). The letters in indicate nonsignificant differences between plants expressing BST4 and their azygous segregants using Tukey post hoc test (P > 0.05). **B.** Non-photochemical quenching (NPQ) as a measure of photoprotection and **C.** photosystem II quantum yield (Y(II)) were recorded during 10 min of illumination at 830 µmol photons m^{-2} s^{-1} followed by a 5-minute dark period. Data are presented as means ± SEM (n=4-6). Asterisks indicate statistical difference between plants expressing BST4 and their Azygous (Az) segregants according to unpaired t-test (P ≤ 0.05). **D.** Proton motive force (PMF) size and **E.** partitioning to pH gradient (ΔpH) after 3 min illumination at 830 µmol photons m^{-2} s^{-1}. Data are means ± SEM (n=5-6). The letters in E and F indicate non-significant differences between plants expressing BST4 and their azygous segregants according to unpaired t-test (P > 0.05).

A. Full length BST4 and homologous sequences

>Brassica_rapa_(PAC:30641593)

----------RTLYTHEKWVEHRSSLRHVHHLFSSFSSRVILSLIPPVFFFTSVAIFIASYNSAVAL----------
DWLPSVFPILR---SSSLPYQLTAPALALLLVFRTEASYSRYEEGRKAWVGIIAGT--
DDLARQVICSVDGSG----------DELVIK-----DLLLRYV----AAFPVALKCHVTYGSD-----VARDLRN---
--LIEGDDLSLI--IESKHR----------PRCVIEFISQSLQL----LKLDDT----------
KRDLLESKMLHLHEGIGVCEQLMGIPIPLAYTRL-TSRFLVFWHLTL-------PIILWDEC-----
HWIVVPATFISAASLFCIEEVGVLIEEPFPM----LALDELCDL-VHSNIQEAVKSES----------
---
>Q9M2D2_-_VCCN1_Athaliana
MY----------QSMNLSVSSNFTHRSLLES----------RFPI-----FSTGFR-----KSVNLKPPRVSSGPE---
SNDSGH----------ETLTDKLIHLLRAVP--------
DWADEIKERGMQQKRSLYTHEKWVEHRSSLRHVRHLLSSFSSRVILSLIPPVFFFTSVAVVIASYNSA
VAL----------DWLPGIFPILR---SSSLPYQLTAPALALLLVFRTEASYSRYEEGRKAWVGIIAGT--
NDLARQVICSVDSSG----------DELIIK-----DLLLRYI----AAFPVALKCHVIYGSD-----IARDLRN-----
LIEADDLSLI--LQAKHR----------PRCVIEFISQSIQL----LKLDDA----------
KRDLLESKMLHLHEGIGVCEQLMGIPIPLSYTRL-TSRFLVFWHLTL-------PIILWDEC-----
HWIVVPATFISAASLFCIEEVGVLIEEPFPM----LALDELCDL-VHSNIQEAVKSEKVIRNRIIAKIKLHEFK--
----HSS----------NGRHRS----------

>Nicotiana_tomentosiformis_(XP_009629643.1)
M----------TNSRTLFSIQSPTNASFSSHF-TLKTPSK--LQQQSFPSKL-
NFKKLRFSTFKVRCCPQ----QTPQN----------QNPTSALISILRIIP--------
DWADRIQEEGMKKKRSLYTHESWMQHRSSLRHVRHLFSSLNSRVILSLVPPVIAFTSVAVVIASYNSA
VSM----------HWLPELFPVLR---ASPLPYQLTAPALALLLVFRTEASYSRFETGKKAWTKVIAGT--
NDFARQVIACVDKS----------DAVLK-----AALLQYI----MAFPVALKCHITYGSD-----IASDLKN-----
LLEADDLAVV--LSSKHR----------PRCIIGFISQCLQS----LHLEGT----------
KLTQLESKISCFHEGIGVCEQLAGIPIPLSYTRL-TSRFLVLWHLTL-------PIILWDDC-----
HWIVVPATFISAASLFCIEEVGVLIEEPFPM----LALDELCQL-
VHDNIQESMANEKKIQERLSAKRKRRFSE------HSQ----------NGWPTS----------
---
>XP_028961536_Malus_domestica
MLLPSSLSLQTLAPPNADTIQKPHQTLPQNLTLFQLVHP------QHFPTLQFPN-----LPSGPKTL-
KFKLLCSQSPNPNPSP-------PSS----------SSPVQTLISILRIIP--------
DWSDRTQERGMRQHRTLYDHEKWMHHRSSYRHLRHLLSSLSSRVILSLIPPVIAFTLVAVVIASYNTA
VAL----------DLLPGIFPLLR---SSSLPYQLTAPALALLLVFRTEASYSRFEEGRKAWTEVIAGA--
NDFARQIISSVETSG----------DAQLK-----KALLQYI----VAFPVALKCHVIYGSD-----IARDLQN-----
LLEVDDLLVV--LNSKHR----------PGCIIQFISRSLQL----LKLEES----------
RRIMLQSKISCFHEGIGICEQLIGTPIPLSYTRL-TSRFLVLWHLTL-------PIILWDDC-----
HWIVVPATFISAASLFCIEQVGVLIEEPFPM----LALDDLCNS-
VRNNVQEALASEKLIRARLAAKGRIQSEQ------QFQ----------NGQPRP----------
---
>Chlamydomonas_eustigma_(GAX83184.1)
M----------LVHRVHTRSLGNRNQCGRK----------
LHRVSTFVVKTPTEKPVVA----
DYVLPRSEEARRYFRTVYDFPQWQKHRSPTRLIDRLLQIPRSHVLQNILPSIAWCSSVAGLLTLYMQA
YDA----------HILPDGFPSFATNNACTSFVNTTTVALSLLLVFRTNVSYGRWDEARKMKGLLVNRS--
RDLMRQVCAMVPEE----------DVATK-----AMMAKWT----AAFCRVLRIHFQPEVS-----LEDEMKG-
----LLSPEELEWL--IESKHR----------PCSVIHMLSQIIYD----SQISAI----------
CQAQMCNNLTAFEDVLGGCERLLRAPIPVSYTRH-TARFLFTWLTLL-------PFALYNSC-----

GVWTLPVVAGVSAVLCGIEEIGVQIEEPFGI----LPLEAICGR-
IQADVMATLKEDAKTRNLRNKVLLIRGPE------HWAMV----------NGHSNK----------
---

>Cre16.g662600.t1.2_(BST1)
M----------QMQA----------NRSSLRASPVRGLGARPLLRALPAGRVARLNVSAQA--
KDPNAPIQ----------SNPLGTLSSQSGQVA----------
TLPRSEEARKYFRTVYDFPQWQKHRSSYRFAERLFQLSQSHILQNALPAISWVTLVATLVASYGYSY
DQ----------HMLPDVFPSISPNASCTAFISNTSVALSLLLVFRTNSSYGRWDEARKMWGGLLNRS--
RDIMRQGATCFPDD----------QVEAK-----KALARWT----VAFSRALRIHFQPEVT-----IESELQN-----
ILTPAELQML--AKSQHR----------PVRAIHAISQIIQS----VPMSSI----------
HQQQMSNNLTFFHDVLGGCERLLRAPIPVSYTRH-TARFLFAWLTLL-------PFALYPTT-----
GWGVVPVCTGIAAVLCGIEEIGVQCEEPFGI----LPLDVICNR-
IQADVMATLKDDADTKTILAEAGLISLIPS----ATSATPVASA----EPVLVSARPSAAPAPNNGLQVRVAM-
----------GG----------ERK*----------

>Cre16.g663400.t2.1_(BST2)
M----------QC----------LSSRPVAMGRAGSSALPRL-
PLRAGRVCHLGVRCQAANKDPNAPIQ----------SNPLGSFSSQLQNQP----------
TLPRSEEARKYFRTVYDFPQWQTHRNQYRLMKRLFSIPQSHVIQNALPSIMWVAFTSTCVAAYMYGY
DQ----------HMLPEGFPTLAPNAACSAFISNTSVALSLLLVFRTNSSYGRWDEARKMWGGLLNRS--
RDIMRQGATCFPDD----------QVEAK-----KALARWV----VAFSRALRIHFQPEVT-----IESELKN-----
ILTPAELQML--AKSQHR----------PVRAIHAISQIIQS----VPMSSI----------
HQQQMSNNLTFFHDVLGGCERLLRAPIPVSYTRH-TARFLFAWLTLL-------PFALYGSC-----
GVSVIPVCSGIAAVLCGIEEIGVQCEEPFGI----LPLDVICNR-
IQADVMATLKDDADTKTILAEAGLISLRA------NSAMAVENALPDLDSINAAAPNGNGSHNGNGAAV-----
----------PVS----------
VSAGA----------
----------SGNGMNV----------RISPR*-----
>Cre16.g663450.t1.2_(BST3)
M----------QVSK----------VPSS------ASARCLPRL-
PVRTSRVCQLSVRCQAANKDPNAPIQ----------SNPLGSFSSQNSSGAVV--------
TAPRNEDARKYFRTVYDFPQWQKHRSQSRLVRRLFTIPQSHVIQNALPSIMWVTFTSTCVAAYMYGY
DL----------HILPEGFPTLAPNAACSAFISNTSVALSLLLVFRTNSSYGRWDEARKMWGGLLNRS--
RDIMRQGATCFPDD----------QVEAK-----KALARWT----VAFARALRIHFQPEVT-----IESELQN-----
ILTPAELQML--AKSQHR----------PVRAIHAISQIIQS----VRMSSI----------
HQQQMSNNLTFFHDVLGGCERLLRAPIPVSYTRH-TARFLFAWLTLL-------PFALYGSC-----
GVSVIPVCTGIAAVLCGIEEIGVQCEEPFGI----LPLDVICNR-IQADVMATLKDDADTKTVLAEAGLISLIP-
-----SMSLPPTEHASPSDPVTAAAAAALAAANGNGAASHSNG----------
----------NG----------SKPVSTQVPP----------PVLAPVTVTS----------
---

>Chlorella_sorokiniana_(PRW33726.1)
M----------STAMLAGSRIQLQQPAG--------LGGSRLQ--RAAAPVAAAA-
RLGSVRPAGLQARSTAARRADRSALR----------VSATASPEAAPVKLS----------
GDDLKEANRKHMRSVFDFDLWKKHRSSSRYLRHIVGLGESRIVSGLMAPLTYVMTLSLAVACYNAAA
EA----------GYLP-VFPELKL--ATNAPFGLTSFALSLLLVFRTNSSYGRWDEARKMWGLIVNRS--
RDFIRQGLGYIPPE----------QEELQ-----KMLVRWT----VAYSRSLMCHLRPGED-----LRVELKD---
--TLKPEELEAL--LASTHR----------PNYVVQVLTAIIKT----
AQLPAAVTNNRDSTGCVPAGAAYRMDENLTVFADVTGGCERILRTPIPLSYTRH-TSRFMMIWLTLL---
----PFTLWDSC-----HWAMLPIAGIVSFLLLGIEEIGVQIEEPFTI----LPLEVISRT-
IEGNVWELYRMHSGEA---LEKEQAELAN------GQDVQVLNA----
QDLVALMAPSAVGNTANGTSRKSLV----------VNYGL----------

>Cre06.g261750.t1.2_(BST4)
M----------QC--------QLKH----------GA-RPQSQRPNWLPARAATLRPAVQHGVR-

----------RGLTLGVKAAAAPLE--------
DKKMPADMTTRQYRRVVYDFALWAKHRDVNRYLYNLRTIPGSRIIRQLSQPMGVVLAWAALFGFYET
CLEA----------GVLPSYLPKMTL--MSAEPQGLTSFALSLLLVFRTNSSYGRFDEARKIWGGILNRA--
RNIANQAVTFIPAE----------DQAGR-----EAVGKWT----VGFTRALQAHLQEDID-----LRKELEKA--
TPRWSKEEIDML--VNAQHR----------PIKAISVLSELTRQ----LSITQF----------
QALQMQENCTFFYDALGGCERLLRTPIPVSYTRH-TARFLTIWLAML-------PLGLWERY-----
HWSMLPVIALIGFLLLGIDEIGISIEEPFGI----LPLDAICGR-
AQTDVNSLLKEDPAVMKYVDDVRSGRVKS------PPPLPPAPA----APAAA-------AAAAAAAARSVSP----
QPDVAKTLGSLFTNVRAGVGAVAPGAPLMPQAPVRSPSPTRSVSP--------
SFPRASAGTGMPPPVGMNG----------ATPRVAAAPPTPPPVSRPAA----------
PAAAPAAGSGFTMPNFSASLSGLTGGAAAAAKSAADAASSKLTKMADSMSSGAAAPAPPAAPAR-----
----------PSTSPRPSASSPISSSADADRSDSSRR---PVNWRDELQSLKATRE----------
PNGNGNGSGVAPAA--GRADADEEALRRFGNLAGRSR----------SGNG----------
GGGSSDTELSEANRPRTRPDWRNQL*
>XP_002945810.1_Volvox_carteri_f._nagariensis
M----------QS--------QLQP----------RL-QLQGTRLNWLPQRSCVQRRSLRVDAT--
----------SG------AAPPPPA--------
GKELSNDMVTRQYRRTVYDFSLWAKHRDVNRYLYNLKTIPGSRIIRTLGQPMGIVLAWAAMFGFYET
CLES----------GVLPSYFPKLTL--MSAEPQGLTSFALSLLLVFRTNSSYGRFDEARKIWGGILNRA--
RNIANQAVTFIPAE----------DVAGR-----EAVGKWA----VGFCRALQAHLQEDAN-----LREELQKA-
-QPRWSREEIDML--CSAQHSWQQLQSCVNAFW-PIKAISMLSELTRQ----LPISQF----------
QALQMQENVTFFYDALGGCERLLRTPIPVSYTRI----------
LPLDAICTR-AQTDVVSLLKDDPAVVKYISDVRQGRIAP------PTEPPVAGA----
APVAAAPPPPPPASAGGGISRSGSPTAQQQPDVMKTVTSMLHNVKAGIGAVAPAPPRPPSPQPRAR
SP-RAASPGGPS----PFPRASAGTG--------G----------
AAAAVPSPPPIKPLTSSSSSSSGAVSKDSNNSTATAKKPASAPAASSA----
GFSMGFSGLADGAAAAAKSAS-AAAAKFSKIADSVVAG--TPAAPASEAKRETAA--AAAMQAQPRN---
TPSSSSSTPSAAPANGSSDDDRSSSGRRTAAAVNWREELAALRAGREDAEEPASASASYDREFPSS
SWSFSSASSAAVVQSGDAEDEARRRFGGLAGRGARSDTTTSAAAVMRGNGNGLSENGYGNGYGN
DN-GNGNGNTVEARGARPRTRPDWRNQL-
>Chrysochromulina_sp._(KOO32217.1)
M----------REHPLSYEEYMRQRS----------AGRDPLA--EAVQGQSASM-
ERGVVPPPPVKATPERTEAAFTPPAEFDFFQDVFKPTVESVVKAVVSPGAQQDSDESYMRVPWWE
QGSTYSEDQRKDRRTVFMHDDWKRHRSSERFFRNIKTWPSSGINQALRKELTFVTSVSVFVVLANM
LLYQYQDFGGVVHPGPLSFLDGPIKSLS---
LPALPFSMASPVLSLLLVFRTNTAYFRWNEARTLWGGLINNC--RNIVRQTTTMFPNDA----------
YHNALK-----KRLATET----ATFIKSLRNFLRGPEDDAT--LRKELYAYVNQGLMTSAQAEAT--LAAKNR---
----------PMFALAAMSATLRK----ANIDEM----------YISRMDSTISVLVDLTGANERIFKSPIPLVYTRL-
TARFLSVFLTLL-------PLAMWAALGESWNHWATIPATFILSVFLFGVEEVGIQIEEPFSI----
LPLEAMCNGAIEAVQLEMLAAE----------QSQVFEAAG----DAVAVA----------
---
>Emiliania_huxleyi_(XP_005770556.1)

--
EFKEAGREFRQDVYSYNDWRWHRESGHIASAISSVFTSGVGKAMWRETFFVIATAAAVYLYNIGVPV
LAAKTAASL----PIVAALLGRLPLLHLSLLPLTLSSPALFLLLVFRTNNSYDRWWEARKVWGGVINAS--
RDLARQALALVR----------DAELK-----KLMVSQI----ASYARVLKYHLGPPTPEARDLLRNELVD--
--NRLPADQVRVI--MEAKHK----------PMALLGLVSASLHDSGR-TGLDTV----------
QASKLDQTLSLLTDYLGKCERIVKTPLPLVYTRH-TARFLSWWLLFL-------PVCLYNQLRA---
NWMIVPVSGLIGFFLVGIEDLGNQIEEPFSI----LPLTAMGTG-IQQSIFEAL----------
---
>Phaeodactylum_tricornutum_(XP_002180738.1)
MM----------RNFASVLLLL-SSGAAAFAPVQHNGVRTIATPSTPLY---
----------GNTKQPPALP--PIK----------
DISYGEESRKYRRTVYSHDDWVKHRSSDRFLRNLLAIGSSGVYKSLAKEVLATTGVATFIVLYNCLVG
GYTDLEGIKHS---ALIESVWAPLMA--LPLAPFTLSSPSLGLLLVFRTNTSYQRWDEARKNWGMNINHT-

-RDLVRMGTSFYDNAA----------VSSEQRAKDL-KALSLAT----WSFVRAMKRHLSPESEDEQD-
FRRELFE-----RLPAPQAQAI--IDAAHR----------PNRALFDLSVAIEN----LPMHFL----------
RKNQVHQAVTIFEDNLGSSERLLTSPVPLFYSRH-TARFLSFWLLLL-------
PFALWDPFAGTWNHVGMIPATAVISIFLFGIEELATQMEEPFTI----LPMQAFCDK-
IGNWCNEIVSWQAGDNGMAVNMPSMISPEGLPELKEPAPVPAMA----
VASVAAAMPVMANGDINGDTTGITM---DQP----------HNAIP----------

>Thalassiosira_pseudonana_(XP_002289965.1)
M----------
GPPIDPSVPVT----------
DQVGEGSRKYRRTVYTHDDWVRHRSPDRFGNNLSTLFNSGIYKQVANEVFATTAVATFVFLWNMIA
GGYTDLAGVQHG---PIIDSPLAQMVG--
LPMTAFTILTPSLGLLLVFRTNTSYGRWDEARKMWGLNINHT--
RDLNRMATAWYGNEGNMDSVAFMGGDIPYSQPIDPVQRAYDL-GQVSLFT----
WAFVRSMKRHLSPPEEDEED-FKAELRA-----RLTPEQAENI--INAAHR----------PNRALFDLSVAIEN--
--LPMHFL----------RKNAINTNLSIFEDTLGGCERLLSSPVPLFYSRH-TARFLSTWLLLL-------
PFGLYEQFKDSWNHIAMIPATAFISVCLFGIEELATQLEEPFTI----LPMQGFCDK-IGGWCDEIVSW-
AGQGQQEYTEENAMSNE------QEMTY----------

----------WR----------

>WP_049046555.1_Kiebsiella_aerogenes

----------MIIRPEQHWFFRLFDWHGSVLSKIVFRLLLNVLMSVIAIISYQWYEQL----------GI------
-----HLTVAPFSLLGIAIAIFLGFRNSASYSRFVEARNLWGTVLIAE--RTLVRQLKNILPD----------
DEETH-----KTLVSYL----VAFSWSLKHQLRK-TD-----PAVDLYR-----LLPKEKVAEI--LASSMP----------
TNRILLLIGNELGRLREQGKLSDI----------TYGLMDNKLDELAHVLGGCERLASTPVPFAYTLI-
LQRTVYLFCTLL-------PFALVGDL-----
HYMTPFVSVFISYTFLSWDSLAEELEDPFGTSANDLPLNAMCNT-
IERNLMDMTGQHPLPEKMQPDRYYNLT----------

>XP_011543531.1_Homo_sapiens
M----------
----------TITYTSQVANARLGSFSRLLLCWRGSIYKLLYGEFLIFLLCYYIIRFIYRLALTEEQQL----------
----MFEKLTL--YCDSYIQL--IPISFVLGFYVTLVVTRW------WNQYENLPWPDRLMSLVSGFVEGK--------
----------DEQGRL--LRRTLIRYANLGNVLILRSVSTAVYKRFP-----SAQHLVQ---
AGFMTPAEHKQLEKLSLPHNM---------FWVPWVWFANLSMKAWLG---GRIRDPI----------
LLQSLLNEMNTLRTQCGHLYAYDWISIPLVYTQVVTVAVYSFFLTCLVGRQFLNPAKAYPGHEL---
DLVVPVFTFLQFFFYVGWLKVAEQLINPFGEDDDDFETNWIVDRNLQVSLLAVDEMHQDLPRMEPDM
YWNKPEP------QPPYTAASA----QFRRASFMGSTFNISLNKEEMEFQPNQEDEED----------
AHAGIIGRFLGLQSHDHHPPRANSRTKLLWPKRESLLHEGLPKNHKAAKQ----
NVRGQEDNKAWKLKAVDAFKSAPLYQRPGYYSAPQ----------TPLSPTPMFFPLEPSA---
PSKLHSVTGI-DTKDKSLKTVSSGAKKSFELLSES--
DGALMEHPEVSQVRRKTVEFNLTDMPEIPENHLKEPLEQSPTNIHTTLKDHMDPYWALENR----------
SVLHLNQGHCIALCPTPASLALSLPFLHNFLGFHHCQSTLDLRPALAWGIYLATFTGILGKC----------
SGPFLTSPWY---HPEDFLGPGEGR----------

B. BST4 and homologous sequences trimmed after the bestrophin domain

>Brassica_rapa_(PAC:30641593)

----------RTLYTHEKWVEHRSSLRHVHHLFSSFSSRVILSLIPPVFFFTSVAIFIASYNSAVAL----------
DWLPSVFPILR---SSSLPYQLTAPALALLLVFRTEASYSRYEEGRKAWVGIIAGT--
DDLARQVICSVDGSG----------DELVIK-----DLLLRYV----AAFPVALKCHVTYGSD-----VARDLRN---
--LIEGDDLSLI--IESKHR----------PRCVIEFISQSLQL----LKLDDT----------

KRDLLESKMLHLHEGIGVCEQLMGIPIPLAYTRL-TSRFLVFWHLTL-------PIILWDEC-----
HWIVVPATFISAASLFCIEEVGVLIEEPFPM----LALDELCDL-VHSNIQEAVKSE
>Q9M2D2_-_VCCN1_Athaliana
MY----------QSMNLSVSSNFTHRSLLES----------RFPI-----FSTGFR-----KSVNLKPPRVSSGPE---
SNDSGH----------ETLTDKLIHLLRAVP--------
DWADEIKERGMQQKRSLYTHEKWVEHRSSLRHVRHLLSSFSSRVILSLIPPVFFFTSVAVVIASYNSA
VAL----------DWLPGIFPILR---SSSLPYQLTAPALALLLVFRTEASYSRYEEGRKAWVGIIAGT--
NDLARQVICSVDSSG----------DELIIK-----DLLLRYI----AAFPVALKCHVIYGSD-----IARDLRN-----
LIEADDLSLI--LQAKHR----------PRCVIEFISQSIQL----LKLDDA----------
KRDLLESKMLHLHEGIGVCEQLMGIPIPLSYTRL-TSRFLVFWHLTL-------PIILWDEC-----
HWIVVPATFISAASLFCIEEVGVLIEEPFPM----LALDELCDL-VHSNIQEAVKSE
>Nicotiana_tomentosiformis_(XP_009629643.1)
M----------TNSRTLFSIQSPTNASFSSHF-TLKTPSK--LQQQSFPSKL-
NFKKLRFSTFKVRCCPQ----QTPQN----------QNPTSALISILRIIP--------
DWADRIQEEGMKKKRSLYTHESWMQHRSSLRHVRHLFSSLNSRVILSLVPPVIAFTSVAVVIASYNSA
VSM----------HWLPELFPVLR---ASPLPYQLTAPALALLLVFRTEASYSRFETGKKAWTKVIAGT--
NDFARQVIACVDKS----------DAVLK-----AALLQYI----MAFPVALKCHITYGSD-----IASDLKN-----
LLEADDLAVV--LSSKHR----------PRCIIGFISQCLQS----LHLEGT----------
KLTQLESKISCFHEGIGVCEQLAGIPIPLSYTRL-TSRFLVLWHLTL-------PIILWDDC-----
HWIVVPATFISAASLFCIEEVGVLIEEPFPM----LALDELCQL-VHDNIQESMANE
>XP_028961536_Malus_domestica
MLLPSSLSLQTLAPPNADTIQKPHQTLPQNLTLFQLVHP------QHFPTLQFPN-----LPSGPKTL-
KFKLLCSQSPNPNPSP-------PSS----------SSPVQTLISILRIIP--------
DWSDRTQERGMRQHRTLYDHEKWMHHRSSYRHLRHLLSSLSSRVILSLIPPVIAFTLVAVVIASYNTA
VAL----------DLLPGIFPLLR---SSSLPYQLTAPALALLLVFRTEASYSRFEEGRKAWTEVIAGA--
NDFARQIISSVETSG----------DAQLK-----KALLQYI----VAFPVALKCHVIYGSD-----IARDLQN-----
LLEVDDLLVV--LNSKHR----------PGCIIQFISRSLQL----LKLEES----------
RRIMLQSKISCFHEGIGICEQLIGTPIPLSYTRL-TSRFLVLWHLTL-------PIILWDDC-----
HWIVVPATFISAASLFCIEQVGVLIEEPFPM----LALDDLCNS-VRNNVQEALASE
>Chlamydomonas_eustigma_(GAX83184.1)
M----------LVHRVHTRSLGNRNQCGRK----------
LHRVSTFVVKTPTEKPVVA----
DYVLPRSEEARRYFRTVYDFPQWQKHRSPTRLIDRLLQIPRSHVLQNILPSIAWCSSVAGLLTLYMQA
YDA----------HILPDGFPSFATNNACTSFVNTTTVALSLLLVFRTNVSYGRWDEARKMKGLLVNRS--
RDLMRQVCAMVPEE----------DVATK-----AMMAKWT----AAFCRVLRIHFQPEVS-----LEDEMKG-
----LLSPEELEWL--IESKHR----------PCSVIHMLSQIIYD----SQISAI----------
CQAQMCNNLTAFEDVLGGCERLLRAPIPVSYTRH-TARFLFTWLTLL-------PFALYNSC-----
GVWTLPVVAGVSAVLCGIEEIGVQIEEPFGI----LPLEAICGR-IQADVMATLKED
>Cre16.g662600.t1.2_(BST1)
M----------QMQA----------NRSSLRASPVRGLGARPLLRALPAGRVARLNVSAQA--
KDPNAPIQ----------SNPLGTLSSQSGQVA----------
TLPRSEEARKYFRTVYDFPQWQKHRSSYRFAERLFQLSQSHILQNALPAISWVTLVATLVASYGYSY
DQ----------HMLPDVFPSISPNASCTAFISNTSVALSLLLVFRTNSSYGRWDEARKMWGGLLNRS--
RDIMRQGATCFPDD----------QVEAK-----KALARWT----VAFSRALRIHFQPEVT-----IESELQN-----
ILTPAELQML--AKSQHR----------PVRAIHAISQIIQS----VPMSSI----------
HQQQMSNNLTFFHDVLGGCERLLRAPIPVSYTRH-TARFLFAWLTLL-------PFALYPTT-----
GWGVVPVCTGIAAVLCGIEEIGVQCEEPFGI----LPLDVICNR-IQADVMATLKDD
>Cre16.g663400.t2.1_(BST2)
M----------QC----------LSSRPVAMGRAGSSALPRL-
PLRAGRVCHLGVRCQAANKDPNAPIQ----------SNPLGSFSSQLQNQP----------
TLPRSEEARKYFRTVYDFPQWQTHRNQYRLMKRLFSIPQSHVIQNALPSIMWVAFTSTCVAAYMYGY
DQ----------HMLPEGFPTLAPNAACSAFISNTSVALSLLLVFRTNSSYGRWDEARKMWGGLLNRS--
RDIMRQGATCFPDD----------QVEAK-----KALARWV----VAFSRALRIHFQPEVT-----IESELKN-----
ILTPAELQML--AKSQHR----------PVRAIHAISQIIQS----VPMSSI----------
HQQQMSNNLTFFHDVLGGCERLLRAPIPVSYTRH-TARFLFAWLTLL-------PFALYGSC-----
GVSVIPVCSGIAAVLCGIEEIGVQCEEPFGI----LPLDVICNR-IQADVMATLKDD
>Cre16.g663450.t1.2_(BST3)
M----------QVSK----------VPSS------ASARCLPRL-
PVRTSRVCQLSVRCQAANKDPNAPIQ----------SNPLGSFSSQNSSGAVV--------
TAPRNEDARKYFRTVYDFPQWQKHRSQSRLVRRLFTIPQSHVIQNALPSIMWVTFTSTCVAAYMYGY

DL----------HILPEGFPTLAPNAACSAFISNTSVALSLLLVFRTNSSYGRWDEARKMWGGLLNRS--
RDIMRQGATCFPDD----------QVEAK-----KALARWT----VAFARALRIHFQPEVT-----IESELQN-----
ILTPAELQML--AKSQHR----------PVRAIHAISQIIQS----VRMSSI----------
HQQQMSNNLTFFHDVLGGCERLLRAPIPVSYTRH-TARFLFAWLTLL-------PFALYGSC-----
GVSVIPVCTGIAAVLCGIEEIGVQCEEPFGI----LPLDVICNR-IQADVMATLKDD
>Chlorella_sorokiniana_(PRW33726.1)
M----------STAMLAGSRIQLQQPAG--------LGGSRLQ--RAAAPVAAAA-
RLGSVRPAGLQARSTAARRADRSALR----------VSATASPEAAPVKLS----------
GDDLKEANRKHMRSVFDFDLWKKHRSSSRYLRHIVGLGESRIVSGLMAPLTYVMTLSLAVACYNAAA
EA----------GYLP-VFPELKL--ATNAPFGLTSFALSLLLVFRTNSSYGRWDEARKMWGLIVNRS--
RDFIRQGLGYIPPE----------QEELQ-----KMLVRWT----VAYSRSLMCHLRPGED-----LRVELKD---
--TLKPEELEAL--LASTHR----------PNYVVQVLTAIIKT----
AQLPAAVTNNRDSTGCVPAGAAYRMDENLTVFADVTGGCERILRTPIPLSYTRH-TSRFMMIWLTLL---
----PFTLWDSC-----HWAMLPIAGIVSFLLLGIEEIGVQIEEPFTI----LPLEVISRT-IEGNVWELYRMH
>Cre06.g261750.t1.2_(BST4)
M----------QC--------QLKH----------GA-RPQSQRPNWLPARAATLRPAVQHGVR-
----------RGLTLGVKAAAAPLE--------
DKKMPADMTTRQYRRVVYDFALWAKHRDVNRYLYNLRTIPGSRIIRQLSQPMGVVLAWAALFGFYET
CLEA----------GVLPSYLPKMTL--MSAEPQGLTSFALSLLLVFRTNSSYGRFDEARKIWGGILNRA--
RNIANQAVTFIPAE----------DQAGR-----EAVGKWT----VGFTRALQAHLQEDID-----LRKELEKA--
TPRWSKEEIDML--VNAQHR----------PIKAISVLSELTRQ----LSITQF----------
QALQMQENCTFFYDALGGCERLLRTPIPVSYTRH-TARFLTIWLAML-------PLGLWERY-----
HWSMLPVIALIGFLLLGIDEIGISIEEPFGI----LPLDAICGR-AQTDVNSLLKED
>XP_002945810.1_Volvox_carteri_f._nagariensis
M----------QS--------QLQP----------RL-QLQGTRLNWLPQRSCVQRRSLRVDAT--
----------SG------AAPPPPA--------
GKELSNDMVTRQYRRTVYDFSLWAKHRDVNRYLYNLKTIPGSRIIRTLGQPMGIVLAWAAMFGFYET
CLES----------GVLPSYFPKLTL--MSAEPQGLTSFALSLLLVFRTNSSYGRFDEARKIWGGILNRA--
RNIANQAVTFIPAE----------DVAGR-----EAVGKWA----VGFCRALQAHLQEDAN-----LREELQKA-
-QPRWSREEIDML--CSAQHSWQQLQSCVNAFW-PIKAISMLSELTRQ----LPISQF----------
QALQMQENVTFFYDALGGCERLLRTPIPVSYTRI----------
LPLDAICTR-AQTDVVSLLKDD
>Chrysochromulina_sp._(KOO32217.1)
M----------REHPLSYEEYMRQRS----------AGRDPLA--EAVQGQSASM-
ERGVVPPPPVKATPERTEAAFTPPAEFDFFQDVFKPTVESVVKAVVSPGAQQDSDESYMRVPWWE
QGSTYSEDQRKDRRTVFMHDDWKRHRSSERFFRNIKTWPSSGINQALRKELTFVTSVSVFVVLANM
LLYQYQDFGGVVHPGPLSFLDGPIKSLS---
LPALPFSMASPVLSLLLVFRTNTAYFRWNEARTLWGGLINNC--RNIVRQTTTMFPNDA----------
YHNALK-----KRLATET----ATFIKSLRNFLRGPEDDAT--LRKELYAYVNQGLMTSAQAEAT--LAAKNR---
----------PMFALAAMSATLRK----ANIDEM----------YISRMDSTISVLVDLTGANERIFKSPIPLVYTRL-
TARFLSVFLTLL-------PLAMWAALGESWNHWATIPATFILSVFLFGVEEVGIQIEEPFSI----
LPLEAMCNGAIEAVQLEMLAAE
>Emiliania_huxleyi_(XP_005770556.1)

--
EFKEAGREFRQDVYSYNDWRWHRESGHIASAISSVFTSGVGKAMWRETFFVIATAAAVYLYNIGVPV
LAAKTAASL----PIVAALLGRLPLLHLSLLPLTLSSPALFLLLVFRTNNSYDRWWEARKVWGGVINAS--
RDLARQALALVR----------DAELK-----KLMVSQI----ASYARVLKYHLGPPTPEARDLLRNELVD--
--NRLPADQVRVI--MEAKHK----------PMALLGLVSASLHDSGR-TGLDTV----------
QASKLDQTLSLLTDYLGKCERIVKTPLPLVYTRH-TARFLSWWLLFL-------PVCLYNQLRA---
NWMIVPVSGLIGFFLVGIEDLGNQIEEPFSI----LPLTAMGTG-IQQSIFEAL---
>Phaeodactylum_tricornutum_(XP_002180738.1)
MM----------RNFASVLLLL-SSGAAAFAPVQHNGVRTIATPSTPLY---
----------GNTKQPPALP--PIK----------
DISYGEESRKYRRTVYSHDDWVKHRSSDRFLRNLLAIGSSGVYKSLAKEVLATTGVATFIVLYNCLVG
GYTDLEGIKHS---ALIESVWAPLMA--LPLAPFTLSSPSLGLLLVFRTNTSYQRWDEARKNWGMNINHT-
-RDLVRMGTSFYDNAA----------VSSEQRAKDL-KALSLAT----WSFVRAMKRHLSPESEDEQD-
FRRELFE-----RLPAPQAQAI--IDAAHR----------PNRALFDLSVAIEN----LPMHFL----------
RKNQVHQAVTIFEDNLGSSERLLTSPVPLFYSRH-TARFLSFWLLLL-------
PFALWDPFAGTWNHVGMIPATAVISIFLFGIEELATQMEEPFTI----LPMQAFCDK-IGNWCNEIVSWQ

>Thalassiosira_pseudonana_(XP_002289965.1)
M----------
GPPIDPSVPVT----------
DQVGEGSRKYRRTVYTHDDWVRHRSPDRFGNNLSTLFNSGIYKQVANEVFATTAVATFVFLWNMIA
GGYTDLAGVQHG---PIIDSPLAQMVG--
LPMTAFTILTPSLGLLLVFRTNTSYGRWDEARKMWGLNINHT--
RDLNRMATAWYGNEGNMDSVAFMGGDIPYSQPIDPVQRAYDL-GQVSLFT----
WAFVRSMKRHLSPPEEDEED-FKAELRA-----RLTPEQAENI--INAAHR----------PNRALFDLSVAIEN--
--LPMHFL----------RKNAINTNLSIFEDTLGGCERLLSSPVPLFYSRH-TARFLSTWLLLL-------
PFGLYEQFKDSWNHIAMIPATAFISVCLFGIEELATQLEEPFTI----LPMQGFCDK-IGGWCDEIVSW-
>WP_049046555.1_Kiebsiella_aerogenes

----------MIIRPEQHWFFRLFDWHGSVLSKIVFRLLLNVLMSVIAIISYQWYEQL----------GI------
-----HLTVAPFSLLGIAIAIFLGFRNSASYSRFVEARNLWGTVLIAE--RTLVRQLKNILPD----------
DEETH-----KTLVSYL----VAFSWSLKHQLRK-TD-----PAVDLYR-----LLPKEKVAEI--LASSMP----------
TNRILLLIGNELGRLREQGKLSDI----------TYGLMDNKLDELAHVLGGCERLASTPVPFAYTLI-
LQRTVYLFCTLL-------PFALVGDL-----
HYMTPFVSVFISYTFLSWDSLAEELEDPFGTSANDLPLNAMCNT-IERNLMDMTGQH
>XP_011543531.1_Homo_sapiens
M----------
----------TITYTSQVANARLGSFSRLLLCWRGSIYKLLYGEFLIFLLCYYIIRFIYRLALTEEQQL----------
----MFEKLTL--YCDSYIQL--IPISFVLGFYVTLVVTRW------WNQYENLPWPDRLMSLVSGFVEGK--------
----------DEQGRL--LRRTLIRYANLGNVLILRSVSTAVYKRFP-----SAQHLVQ---
AGFMTPAEHKQLEKLSLPHNM---------FWVPWVWFANLSMKAWLG---GRIRDPI----------
LLQSLLNEMNTLRTQCGHLYAYDWISIPLVYTQVVTVAVYSFFLTCLVGRQFLNPAKAYPGHEL---
DLVVPVFTFLQFFFYVGWLKVAEQLINPFGEDDDDFETNWIVDRNLQVSLLAVDEMH

Supplemental Figure 12. Sequences used to generate MAFFT alignments used to generate the phylogenetic trees included in this manuscript. FASTA files of MAFFT alignments of **A.** Full length and **B.** trimmed after the bestrophin domain BST4 and homologous amino acid sequences.